Contents lists available at ScienceDirect

Lithos

Restoration of Late Neoarchean–Early Cambrian tectonics in the Rengali orogen and its environs (eastern India): The Antarctic connection

A. Bhattacharya [a,*], H.H. Das [a], Elizabeth Bell [b], Atreyee Bhattacharya [c], N. Chatterjee [d], L. Saha [e], A. Dutt [e]

[a] Department of Geology and Geophysics, Indian Institute of Technology, Kharagpur 721 302, India
[b] Department of Earth and Space Sciences, University of California Los Angeles, 595 Charles Young Drive East, Los Angeles, CA 90095, USA
[c] Environmental Studies, Institute of Arctic and Alpine Research (INSTAAR), University of Colorado Boulder, 4001 Discovery Drive, Boulder, CO 80303, USA
[d] Department of Earth, Atmospheric & Planetary Sciences, Massachusetts Institute of Technology Cambridge, MA 02139, USA
[e] Department of Earth Sciences, Indian Institute of Technology, Roorkee, Uttarakhand 247 667, India

ARTICLE INFO

ABSTRACT

Geological mapping and P–T path reconstructions are combined with monazite chemical age and Secondary Ion Mass Spectrometric (SIMS) U–Pb zircon age determinations to identify crustal domains with distinctive evolutionary histories in the Rengali orogen sandwiched between two Grenvillian-age metamorphic belts, i.e. the Eastern Ghats Granulite Belt (EGGB) in the south, and the amphibolite facies Gangpur Schist Belt (GSB) in the north, which in turn forms a collar along the NW/W margins of the Paleo/Mesoarchean Singhbhum Craton (SC) north of the Rengali orogen. Anatectic gneisses in the orogen core exhibit multi-phase Neoarchean/Paleoproterozoic deformation, metamorphic P–T histories and juvenile magma emplacement events. The high-grade belt is inferred to be a septum of the Bastar Craton (BC). The flanking supracrustal belt in the orogen — dominated by quartz-muscovite schists ($\pm$ staurolite, kyanite, garnet pyrophyllite), inter-bedded with poorly-sorted and polymict meta-conglomerate, and meta-ultramafic/amphibolite bands — evolved along P–T paths characterized by subgreenschist to amphibolite facies peak P–T conditions in closely-spaced samples. The supracrustal rocks and the anatectic gneisses of contrasting metamorphic P–T histories experienced D_1, D_2 and D_3 fabric-forming events, but the high-angle obliquity between the steeply-plunging D_3 folds in the anatectic gneisses and the gently-plunging D_3 folds in the supracrustal unit suggests the two lithodemic units were tectonically accreted post-S_2. The supracrustal belt is inferred to be a tectonic mélange formed in an accretionary wedge at the tri-junction of the Bastar Craton, the Eastern Ghats Granulite Belt and the Singhbhum Craton; the basin closure synchronous with the assembly of EGGB and the Singhbhum Craton–Gangpur Schist belt composite occurred between 510 and 610 Ma. Based on the available evidence across the facing coastlines of the Greater India landmass and the Australo–Antarctic blocks at ~500 Ma, it is suggested that the EGGB welded with the Greater India landmass during the Pan African along an accretion zone, of which the Rengali orogen is a part, synchronous with the final assembly of the Gondwanaland.

1. Introduction

Accretionary orogens comprise crustal domains having different composition, age, evolutionary history, thermal structure and rheological anisotropy (Cook and Royden, 2008; Klemperer, 2006; Lee et al., 2012a). In the accretion zones, the crustal domains are often intricately interleaved, and their identities partly obscured by ductile flow (Jamieson et al., 2007), anatectic melting especially in deeply-eroded orogen (Northrup, 1996; Williams and Hanmer, 2006), and chemical–mineralogical modifications induced by fluid permeation along structurally-controlled conduits (Koons et al., 1998; Lyubetskaya and Ague, 2010). A critical analysis of the evolutionary histories of the disparately-evolved crustal domains is crucial for tectonic restoration of these orogens and in understanding the dynamics of the accretion processes.

The WNW-trending Rengali orogen (Chetty, 2014; Crowe et al., 2001, 2003; Nash et al., 1996) in eastern India is sandwiched between the Paleo/Mesoarchean Singhbhum Craton (SC) and the enveloping Gangpur Schist Belt (GSB) in the northwest, and the Neoproterozoic domain of the Eastern Ghats Belt (EGGB) dominated by ultra-high temperature granulite facies gneisses in the south (Fig. 1). The orogen comprises anatectic high-grade gneisses and greenschist/amphibolite facies supracrustal rocks, the latter deemed to unconformably overlie the high grade gneisses (Mahalik, 1994). The orogen evolved by transpressional deformation as a result of oblique collision between

* Corresponding author. Tel.: +91 9434743228 (handset).
 E-mail address: abbhat55@gmail.com (A. Bhattacharya).
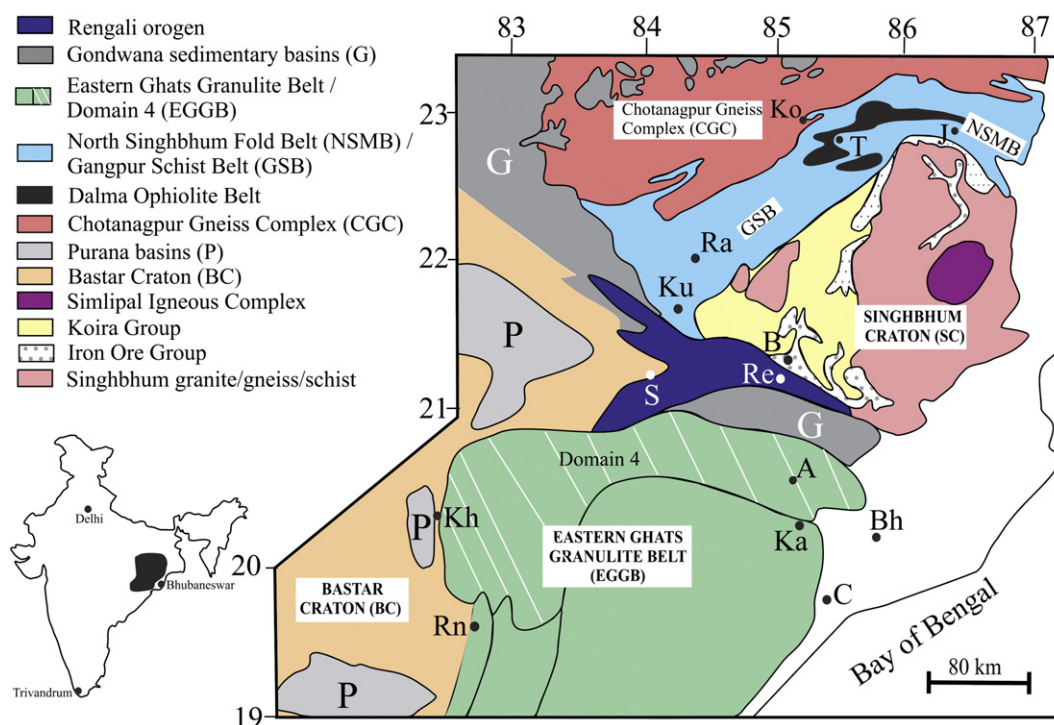
Fig. 1. Simplified geological map of eastern India showing the Rengali orogen sandwiched between the Neoproterozoic domain (domain-4 of Rickers et al., 2001) of the Eastern Ghats Granulite Belt (EGGB), and the Singhbhum Craton and the flanking Gangpur Schist Belt (GSB) in the north. The map is modified after Crowe et al. (2003), Rickers et al. (2001) and the Deogarh Quadrangle map (2003). Acronyms of places: A — Angul; B — Barkote; Bh — Bhubaneswar; C — Chilka; J — Jamshedpur; Ka — Kantilo; Kh — Khariar; Ko — Kolomda; Ku — Kuchinda; Ra — Rajgangpur; Re — Rengali; Rn — Ranmal; S — Sambalpur; T — Tebo. CGC: Chottanagpur Gneiss Complex.

the Singhbhum Craton and the EGGB granulites (Bhattacharya, 1997, 2002; Ghosh et al., 2016; Mishra and Gupta, 2014; Misra et al., 2000).

Based on zircon (SHRIMP) ages obtained from high grade gneisses in the Rengali orogen, Bose et al. (2013) suggest the existence of a marine basin south of the Singhbhum craton at ca. 3050 Ma; according to the authors, the basin closure, marked by the Rengali Orogeny, occurred during the Neoarchean (~2.8 Ga) and is correlated with the southward growth of the Singhbhum craton. The record of Late Neoproterozoic/ Early Paleozoic monazite overprinting in the rocks is correlated by the authors to tectonic rejuvenation, but details of this Pan African tectonism is lacking. Based on LA-ICP-MS zircon ages Chattopadhyay et al. (2015) suggest the Rengali supracrustal rocks to have been deposited between 2.79 and 2.42 Ga on the ~2.80 Ga Pal Lahara gneiss basement. Several Neoproterozoic zircon/monazite age populations (0.98–0.94 Ga, 0.85–0.80 Ga and 0.62–0.50 Ga) common between the Eastern Ghats Granulites and the Rengali supracrustal unit led Chattopadhyay et al. (2015) to infer that the eventual docking (Rengali orogeny) of the Eastern Ghats Granulite Belt and the "cratonic India" was of Grenvillian-age, and not during the Pan African as has been suggested by several authors (Biswal et al., 2007; Das et al., 2008; Dobmeier et al., 2006; Simmat and Raith, 2008). Ghosh et al. (2016) infer that the transpressive deformation in the Rengali orogen was Pan African in age.

Several aspects are crucial to the debate on the age of Rengali orogeny. First, it is necessary to ascertain if the high-grade anatectic gneisses in the Rengali orogen constitute a septum of the Bastar Craton (Fig. 1) extending eastwards into the Rengali orogen (cf. Mishra and Gupta, 2014), or if this lithodemic unit constitutes the southward growth of the Singhbhum Craton (Bose et al., 2013). Second, it is imperative to deduce if the greenschist/amphibolite facies supracrustal unit flanking the gneissic core in the Rengali orogen unconformably overlies the gneisses (Mahalik, 1994), or if the supracrustal unit was accreted to the gneissic domain (Ghosh et al., 2016). And finally, the Rengali orogen reorients the deformation fabrics in the Gangpur Schist Belt, and therefore, the age of the Rengali orogeny is likely to be better constrained once the

structural, metamorphic and chronological history of the Gangpur Schist Belt are known. In this study, we provide the results of lithostructural mapping in the orogen and its neighboring domains, and P–T path reconstructions in selected lithodemic units. These findings are integrated with Secondary Ion Mass Spectrometry (SIMS) U–Pb zircon dating of gneisses within the orogen and U–Pb–Th chemical age determinations in monazites in the different lithodemic units to reconstruct the age and the tectono-thermal setting of the Rengali orogen, and constrain the age of the final assembly of the Greater India landmass in the context of Gondwanaland formation.

2. Lithological set-up of the Rengali orogen

The WNW-trending Rengali orogen (Fig. 2a) comprises three lithodemic units, i.e. the anatectic high-grade anatectic gneisses, supracrustal rocks, and granitoids. The anatectic gneisses (Fig. 3a, b) in the core of the orogen are flanked by greenschist/amphibolite facies supracrustal belts. The northern and southern supracrustal belts converge in the ESE and arguably constitute two limbs of a regional fold (Fig. 2a). Foliated granitoids (broadly granodiorite-granite in composition) with intensely sheared margins (Fig. 3c) with gneisses and schists commonly host enclaves of the anatectic gneisses (Fig. 3d), but enclaves of supracrustal rocks are lacking in the granitoids.

The northern limb of the Rengali supracrustal belt is dominated by quartzite, micaceous quartzite and muscovite schist (staurolite, kyanite, garnet, kaolinite, pyrophyllite occur sporadically) and intra-formational conglomerates that are inter-banded with ultramafic schists (tremolite, antigorite ± anthophyllite, with modally subordinate sphene, minor albite), and aerially subordinate amphibolites (hornblende–plagioclase–epidote–sphene ± garnet). The belt is sandwiched between the Rengali anatectic gneisses in the south, and the lithologies of the Gangpur Schist Belt (GSB) and the Singhbhum Craton (SC) in the north (Fig. 2a). The northern margin of the supracrustal belt is demarcated by a ~2 km wide shear zone (coinciding with the
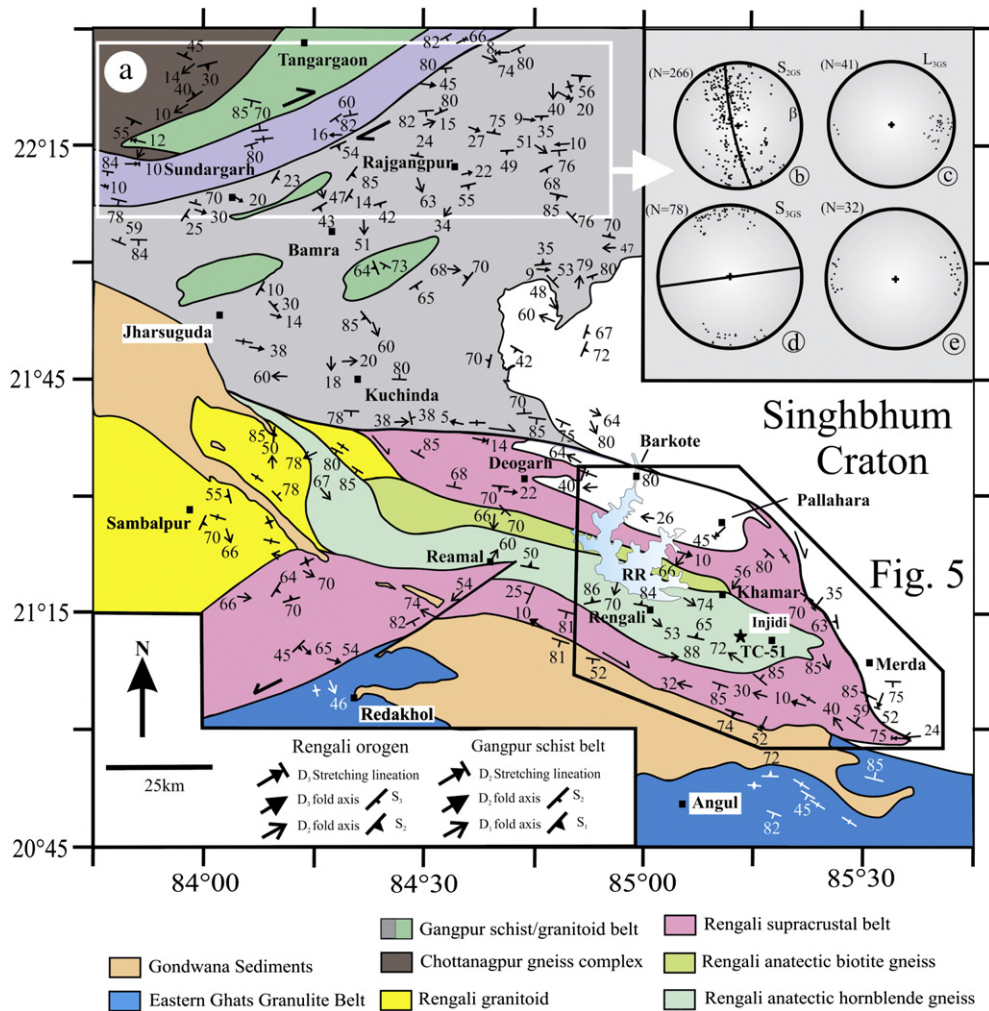
Fig. 2. (a) Litho-structural map of the Rengali orogen and the neighboring crustal domains. S_2, D_2 fold axis in the anatectic gneisses and the supracrustal belt within the Rengali orogen are not time equivalent. Note same symbols are chosen for mesoscale structures, i.e. S_2 and S_3, D_2 and D_3 fold axes, and D_3 stretching lineations, in the Gangpur Schist Belt and in the lithodemic units in the Rengali orogen, and the EGGB, but these structures are not time-equivalent (see text for detailed discussion). The Gondwana sedimentary basin is modified after the Deogarh Quadrangle map (2003). RR — Rengali reservoir. (b–e) Stereographic projections of meso-scale structures correspond to the area shown in white box (with arrow) in the Gangpur schist belt: (b) Poles to S_{2GS} schistosity; (c) plunge of F_{3GS} folds; (d) poles to S_{3GS}; girdle shows mean orientation of S_{3GS}. (e) D_{3GS} stretching lineations in granite mylonite. N = number of data. The mesoscale structures in the Rengali gneisses and schists, and the sheared granites of the Singhbhum Craton neighboring the Barkote shear zone shown in Fig. 5 are from the area outlined in polygonal box, with Fig. 5 keyed to the box. Locations of samples used for metamorphic P–T estimation are in Appendix A.

Barkote shear zone; Crowe et al., 2003) passing south of Kuchinda, north of Deobhog, and extending to Kamakhyanagar in the east. Deformed quartz pebble/cobble and polymict conglomerates are common along the contact between the supracrustal belt and the GSB-SC lithologies. The schist belt tapers out westwards and eventually disappears in the WNW where the Rengali anatectic gneisses are directly juxtaposed with the Gangpur Schist Belt (Fig. 2a). Along the northern margin of the Rengali orogen, the NE/ENE-trending steep-dipping foliation in the Gangpur schists is drawn into parallelism with the WNW-trending Rengali supracrustal belt (Fig. 2a).

The southern limb of the Rengali supracrustal belt is lithologically similar to the northern schist belt, but conglomerates and ultramafic schists are rare. The southern schist belt is sandwiched between the Rengali high-grade gneisses and the Sambalpur granitoid body in the north, and the EGGB in the south dominated by garnetiferous blastoporphyritic granitoids and anatectic quartzofeldspathic gneisses (terminology after Mukhopadhyay and Bhattacharya, 1997), calc-silicate and mafic granulites, and garnet-sillimanite gneisses. The arcuate Kerajangi Fault Zone (Crowe et al., 2003) limits the northern margin of the EGGB (Fig. 2a).

3. P–T-deformation history of the Gangpur Schist Belt

3.1. Structural set-up

Chaudhuri and Pal (1977, 1982) and Chaudhuri et al. (1980) reconstructed the stratigraphy and the superposed fold geometry of the ENE-trending Gangpur Schist Belt (Banerjee, 1967; Kanungo and Mahalik, 1975) around Rourkela located in the NE of the area shown as white box in Fig. 2a. But the P–T-deformation–time (t) history of the Gangpur Schists is unknown. The GSB is dominated by muscovite–biotite schist, banded and micaceous quartzite, metamorphosed marl and dolomite, and talc–tremolite schist intruded by ENE-trending lenses of coarse-grained tourmaline-bearing granites. The penetrative fabric in the schists is a crenulation cleavage S_{2GS}, with the earlier schistosity (S_{1GS}) preserved as microfolds in S_{2GS} interfolial domains, and in pre-S_{2GS} garnet, staurolite and biotite porphyroblasts. The S_{2GS} schistosity describes open, upright and asymmetric folds (F_{3GS}; Fig. 2b) plunging at gentle to moderate angles towards ENE and WSW (Fig. 3e; Fig. 2c). The F_{3GS} folds become increasingly crenulated northwards, develop prominent non-cylindricity (eye-shaped folds in horizontal section), and are axial
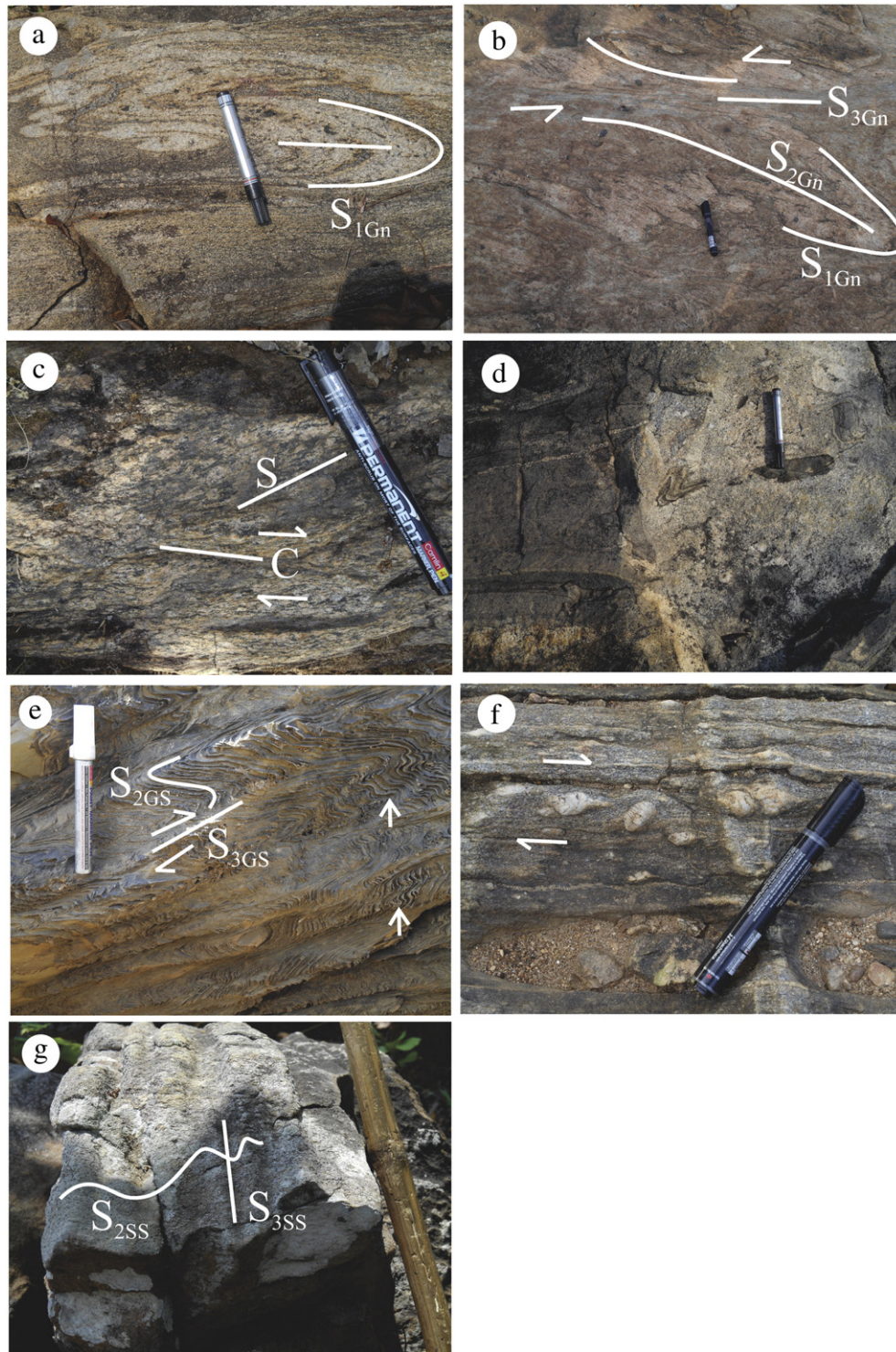
Fig. 3. Field photos of (a, b) Rengali anatectic gneisses, (c, d) Rengali foliated granites, (e) Gangpur calcareous schist, (f) granite mylonite north of GSB, and (g) mica schists in the Rengali supracrustal belt. (a) Isoclinal D_{2Gn} folds on S_{1Gn} leucosomes; note the thickened hinges and strongly attenuated limbs of the D_{2Gn} folds. (b) S_{1Gn}, S_{2Gn} and S_{3Gn} fabrics in anatectic gneisses. Note sinistral sense of shearing along S_{3Gn}. (c) S–C fabrics showing dextral sense of shear in granite mylonite, south of Kuchinda. (d) Enclaves of gneisses within deformed Rengali granite (intrusive into the gneisses). (e) Non-cylindrical asymmetric F_{3GS} folds (arrows) developed on penetrative S_{2GS} schistosity in the Gangpur calc-schists. Note spaced nature of S_{3GS} crenulation cleavage in the schist. (f) Clasts of K-feldspar porphyry in granite mylonite (north of Sundergarh) showing dextral sense of shear along D_{2GS} shears. (g) Profile section (looking west; width of photo 3 m) of gently-plunging asymmetric D_{3SS} fold on S_{2SS} schistosity in micaceous quartzite in Rengali supracrustal belt.

planar to steep-dipping ENE-trending axial planar schistosity, S_{3GS} (Fig. 3e; Fig. 2d) that evolve into a mylonitic fabric northwards. The schists terminate against intensely-sheared and mylonitized blastoporphyritic granitoids containing δ-, σ- and winged-clasts of former K-feldspar porphyries (Fig. 3f). The intensity of the mylonite fabric in the deformed granites ($\approx S_{3GS}$ in the schists) wanes northwards,

where it is manifested by weakly-deformed/un-deformed porphyritic granite; across the ~20 km wide ENE-trending shear zone, the granitoid body gives way to a host of gneisses and schists of the Chottanagpur Gneiss Complex (CGC). The asymmetry of the clasts and the macroscopic S–C fabric orientations in the granite mylonites suggest an apparent dextral sense of movement on the plane of shearing (Fig. 3f). In the

granite mylonites, stretching lineations defined by quartz ribbons and feldspar clasts/augen is sub-horizontal (Fig. 2e). The structural features suggest shearing was dominated by dip-slip sense of movement on the shear plane (cf. Ghosh et al., 2003).

3.2. P–T path reconstruction

The P–T evolutionary history of the Gangpur schists was obtained for a garnet-staurolite bearing mica schist (J-54; mineral analyses in Supplementary Material 1). The S_{2GS} schistosity in the rock (Fig. 4a) is defined by shape-preferred aggregates of muscovite [Si = 3.08–3.11 per formula unit], biotite [X_{Fe}: (Fe/Fe + Mg) = 0.61–0.57], quartz lentils, minor chlorite and ilmenite. The rock is dotted with numerous syn/post-S_{2GS} garnet porphyroblasts, and fewer syn-S_{2GS} staurolite porphyroblasts replaced along margins by post-S_{2GS} chlorite [XFe: Fe/Fe + Mg) = 0.57–0.59], (Fig. 4a–c). The staurolite and garnet porphyroblasts nucleate and grow irrespective of each other, i.e. the two minerals do not share a reaction relationship, although at places, the garnets are partly enclosed within staurolite (Fig. 4b). The garnet porphyroblasts are zoned (Figs. 4b–e); the porphyroblasts exhibit a rimward decrease in X_{Ca}^{Grt} ($= Ca/Ca + Mg + Fe$) from 0.05 to 0.01 and X_{Mn}^{Grt} ($= Mn/Mn + Mg + Fe + Ca$) from 0.08 to 0.02, with a complementary increase in X_{Fe} ($= Fe/Mn + Mg + Fe + Ca$) from 0.81 to 0.90, but Fe/Fe + Mg in garnet decreases only marginally from 0.94 to 0.92 (Fig. 4d, e). The zoning profiles in the garnet porphyroblasts hosted within staurolite and those occurring exclusive of staurolite exhibit similar patterns (Fig. 4d, e).

A MnCKFMASH P–T pseudosection was constructed (Fig. 4f) using the Perple_X program (details in Appendix B). Quartz and H_2O were assumed to be in excess. In the P–T pseudosection, X_{Ca} and X_{Mn} in garnet decrease with increasing P, T within the biotite–chlorite–muscovite–staurolite–garnet field (Fig. 4f), and the isopleths of X_{Fe}^{Grt} — inclined at low angle to the pressure axis — decrease with increasing temperature (Fig. 4f). In the higher-T staurolite–muscovite–biotite–garnet field, all the three compositional parameters decrease with increasing P, T, but in the lower-T chlorite–muscovite–staurolite–garnet field, the three garnet isopleths are sub-parallel to the P-axis, and decrease with increasing pressure (Fig. 4f). The P–T trajectory experienced by the rocks consistent with the garnet zoning profile suggests the GSB crustal domain experienced near-isothermal loading in the chlorite–muscovite–biotite–staurolite–garnet field (Fig. 4f). The P–T range is similar with the P–T values (4–6 kbar, 450–510 °C) retrieved from several formulations of biotite-garnet thermometers (Ferry and Spear, 1978; Hodges and Spear, 1982; Ganguly and Saxena, 1984; Indares and Martignole, 1985; Bhattacharya et al., 1992), and the garnet-muscovite-biotite-plagioclase barometer of Hodges and Crowley (1985). The post-S_{2GS} stabilization of chlorite replacing staurolite (Fig. 4b) and thin Ca-richer collars in garnet (Fig. 4c) suggest cooling-decompression in the retrograde sector of a counterclockwise P–T path.

4. P–T-deformation history of garnet-biotite anatectic gneisses in the Rengali orogen

4.1. Structural set-up

The anatectic gneisses may be grouped in two mineralogical varieties, i.e. (i) pyroxene (Cpx ≫ Opx), hornblende (with modally minor amount of biotite), plagioclase, K-feldspar and quartz bearing gneisses,
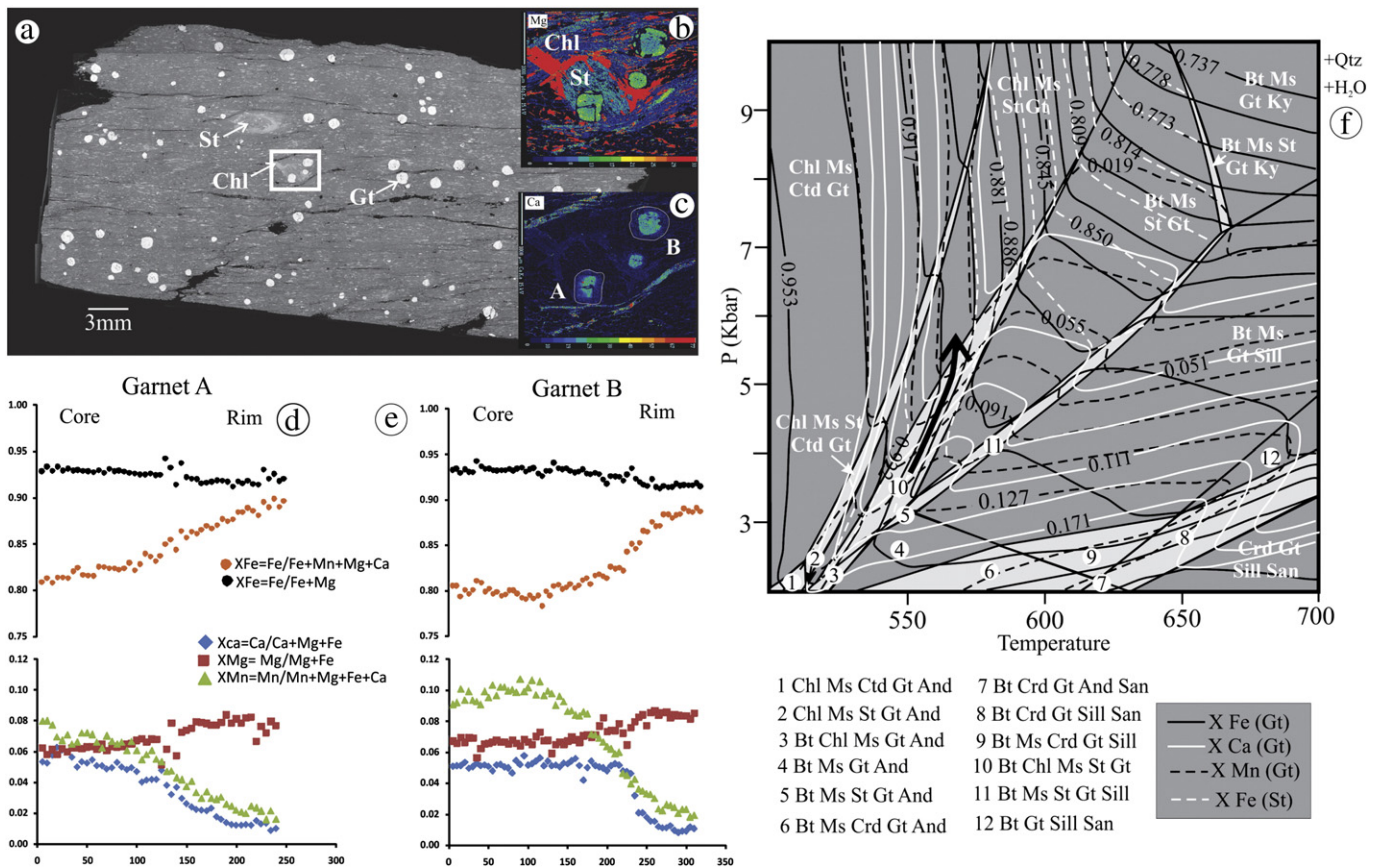
Fig. 4. P–T path reconstruction in Gangpur schist, J-54 (location in Appendix A). (a) Back scattered electron (BSE) image of thin section of J-54 showing the occurrence of garnet and staurolite porphyroblasts in biotite-muscovite-chlorite matrix. (b, c) X-ray element maps of box in 'a' showing chemical zoning in (b) Mg and (c) Ca in garnets A and B. (d, e) core to rim compositional variations in garnet A hosted within staurolite (d) and garnet B in the matrix (e). MnCKFMASH P–T pseudosection constructed for J-54 showing the possible prograde metamorphic P–T path along which the rock evolved. Whole rock composition: e.g. $SiO_2 = 64.24$: $Al_2O_3 = 17.12$; $TiO_2 = 0.73$; FeO = 6.13; MnO = 0.08; MgO = 1.63; CaO = 0.09; $Na_2O = 1.03$; $K_2O = 3.54$; $P_2O_5 = 0.05$ and H_2O (LOI) = 3.48 (Total = 98.12). All values in wt.%.

with garnet mostly occurring intergrown with quartz, and forming coarse mantles at the interface of polygonized grains of hornblende/clinopyroxene and plagioclase); and (ii) biotite-bearing ($\pm$ sillimanite $\pm$ cordierite) gneisses that contain profuse porphyroblasts of garnet both in the melanosome and in the leucosome layers. In these gneisses, the leucocratic layers rimmed by selvages of ferromagnesian phases (e.g. hornblende in the orthogneisses, and biotite in the paragneisses) are the earliest tectonic fabric (S_{1Gn}: D_{1Gn} deformation) (Fig. 3a, b). The S_{1Gn} layers are thickened at the hinges of these tight to isoclinal F_{2Gn} fold, and are strongly attenuated and distended in the fold limbs (Fig. 3a). Syn/post-D_{2Gn} leucosomes are lacking in the gneisses. The D_{2Gn} folds are associated with a penetrative axial plane foliation, S_{2Gn} (Fig. 3a, b). S_{1Gn}–S_{2Gn} intersection lineations in the gneisses are steeply-plunging (Fig. 5a). In regional scale, the steep-dipping S_{1Gn}∥S_{2Gn} fabrics (Fig. 5a) in the gneisses have variable orientations (Fig. 3b). However, in outcrop scale, the axial planar fabric corresponding to the open F_{3Gn} folds is sparsely developed, but S_{3Gn} fabrics are well-developed neighboring the WNW-trending D_{3Gn} shear zones (Fig. 3b). D_{3Gn} stretching lineation plunge moderately towards southwest (Fig. 5e). The sub-vertical β-axis of the poles to the S_{2Gn} broadly overlaps with the mean orientation of the S_{1Gn}–S_{2Gn} intersection lineations (Fig. 5a). This implies that the steeply-plunging F_{2Gn} and the F_{3Gn} folds were broadly coaxial.
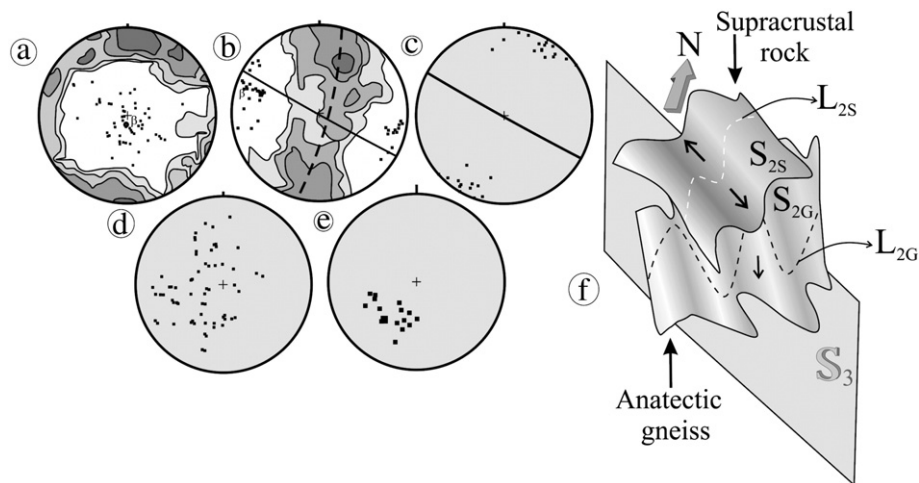
4.2. P–T path reconstruction

The P–T history of the anatectic orthogneisses are discussed in Bose et al. (2014). In this section, we focus on the P–T history of the anatectic garnet-biotite gneisses. The gneisses may be grouped into two mineralogical varieties, i.e. biotite-rich ($+$ sillimanite $+$ K-feldspar $+$ quartz $\pm$ cordierite) melanocratic layer alternating with quartz-syenite leucocratic layers (Fig. 6a, b), and biotite-rich ($+$ plagioclase $+$ K-feldspar $+$ quartz) melanocratic layers alternating with quartz-tonalite layers. The mineralogical difference between the two lithologies is reflected in the bulk compositions of J-416B (K-richer sillimanite-bearing gneiss) and J-468 (Na, Ca-richer sillimanite-free gneiss).

In the gneisses, garnets are chemically homogenous (Fig. 6c, d) and occur both in the leuco- and melano-cratic layers (Fig. 6a, c). In any rock, the garnets are chemically similar in both the layers. In the sillimanite-bearing gneiss, garnets are generally inclusion-free (Fig. 6b); by contrast, garnets in the sillimanite-free gneisses are studded with poly/mono-mineralic inclusions of K-feldspar, quartz, plagioclase, biotite and ilmenite. In the melanocratic layer, garnets overgrow the S_{2Gn} fabric (Fig. 6a). Cordierite in the sillimanite-bearing gneiss occurs as xenomorphic grains within the biotite–sillimanite aggregates overgrowing the S_{2Gn} fabric (Fig. 6b). In the sillimanite-bearing gneiss, Na-rich plagioclase occurs as rare lamellae within K-feldspar porphyries in leucosome, and as thin blebs at the interfaces of melano- and leucocratic layers (Fig. 6a, b). By contrast, in the sillimanite-free gneisses, plagioclase occurs as coarse porphyries in the leucosomes and as polygonized grains in the biotite-rich melanocratic mosaic. Orthopyroxene is typically absent in these gneisses. However, orthopyroxene is restricted to rare garnetiferous charnockite lenses within the gneisses.

The KFMASH phase topology and the relevant X_{Fe} [$= Fe/Fe + Mg$] isopleths in biotite, garnet and cordierite (Fig. 6e; mineral analytical data in Supplementary Material 2) was constructed for J-416B using wt.% H_2O constrained by the loss on ignition (LOI) value. The small amounts of CaO and Na_2O are ignored in the computations. The convergence of X_{Fe} [$Fe/Fe + Mg$] isopleths in garnet (0.80–0.82) and biotite (0.42–0.43) suggest that the pre/syn-S_{1Gn} prograde melting occurred at T > 800 °C and P > 7 kbar via the reaction biotite + sillimanite + K-feldspar → garnet + melt. The peak-P, T conditions are consistent with the P–T values (700–950 °C, 8–10 kbar) obtained from Opx–Grt–Plag–Qtz assemblage in the associated charnockite, J-469 (Fig. 6f; analytical data in Supplementary Material 3). The T_{max} values (850–950 °C) retrieved from Al-in-Opx thermometer (Aranovich and Berman, 1997) are higher by 100–150 °C compared to temperatures retrieved using Fe–Mg exchange thermometers (Bhattacharya et al., 1991; Harley, 1984; Lee and Ganguly, 1988; Sen and Bhattacharya, 1984). However, for any thermo-barometric formulation, T and P values retrieved using rim and core compositions of orthopyroxene, garnet and plagioclase lie within the ± 50 °C and ± 1 kbar errors in the thermo-barometric formulations. In the retrograde sector of the clockwise P–T path (Fig. 6e), post-S_{2Gn} cordierite (X_{Fe}: 0.26–0.30) was stabilized at the expense of biotite and sillimanite via the model reaction, biotite + sillimanite → cordierite + K-feldspar [2 K(Mg, Fe)$_3$AlSi$_3$O$_{10}$(OH)$_2$ + 6Al$_2$SiO$_5$ + 9SiO$_2$ → 3(Mg,

(In wt.%)	SiO$_2$	TiO$_2$	Al$_2$O$_3$	FeO	MnO	MgO	CaO	Na$_2$O	K$_2$O	P$_2$O$_5$	H$_2$O (LOI)	Total
J-416B	65.64	1.08	12.86	11.11	0.06	3.00	0.69	0.94	3.66	0.03	0.91	99.98
J-468	66.31	0.77	13.79	8.54	0.07	1.80	3.00	2.30	1.90	0.15	0.60	99.23

Fig. 5. Stereographic projections (a–e; n = number of measurements) of mesoscale structures in anatectic gneisses and supracrustal rocks in the Rengali orogen, Fig. 2a. (a) D_{2Gn} fold axis lineations, L_{2Gn} (filled square; n = 55), poles to S_{2Gn} foliation (contoured; n = 107), and the β-axis, L_{3Gn} (82/183 N) of S_{2Gn} pole girdle in anatectic gneisses. (b) Contoured poles to S_{2SS} foliation in the supracrustal rocks (n = 181), and D_{3SS} fold axes, L_{2SS} (filled squares; n = 47) in the supracrustal rocks. The β-axis, L_{3SS} (09/285) of the mean S_{2SS} pole girdle (broken line), and the mean S_{3S} plane (continuous line, see c) are shown for reference. (c) Poles to S_{3SS} (filled squares; n = 47) and the mean S_{3SS} plane (210/50 W) in the supracrustal rocks. (d) D_{2SS} fold axis lineations (n = 65) in the supracrustal rocks. (e) Stretching lineations (n = 18; mean orientation 44/255 N) from the northern shear zone. (f) Cartoon showing contrasts in D_3 fold axes, L_3 (thin arrows) and orientations of L_2 lineations (broken lines) in anatectic gneisses and supracrustal rocks. The orientation of WNW-trending S_3 plane ($S_{3Gn} \approx S_{3SS}$) is shown.
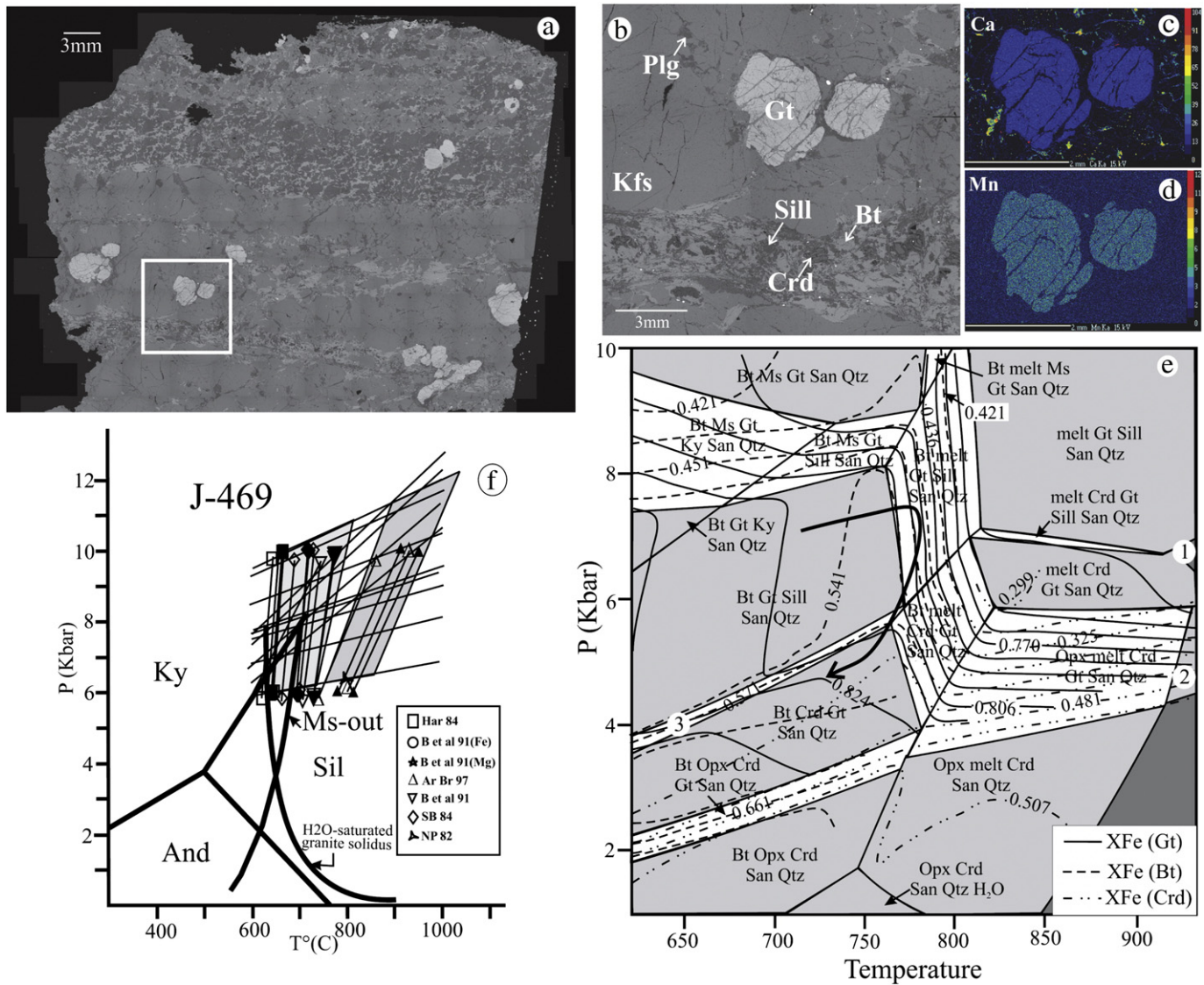
Fig. 6. P–T path reconstruction in anatectic garnet-biotite gneiss, J-416B (location in Appendix A). (a) BSE image of thin section J-416B showing the occurrence of garnet in biotite-poor quartz + K-feldspar leucosome and biotite-rich melanosome layers. (b) Close up BSE image of box in 'a' showing the occurrence of cordierite and sillimanite in the melanosome layer. Note plagioclase occurs as veinlets at K-feldspar grain/sub-grain margins and at leucosome/melanosome interface. (c, d) Ca and Mn X-ray maps emphasize the chemically homogenous nature of the garnets in spite of their large sizes; (e) KFMASH P–T pseudosection (bulk rock composition in text) constructed for J-416B showing the possible P–T path along which the rock evolved. (f) P–T conditions obtained from orthopyroxene-garnet-plagioclase-quartz assemblage in charnockite J-469 (location in Appendix A; analytical data in Supplementary Material 3). Acronyms: Har 84 (Harley, 1984); B et al. 91(Fe), B et al. 91 (Mg) and B et al. 91 (Bhattacharya et al., 1991); Ar Br 97 (Aranovich and Berman, 1997); SB 84 (Sen and Bhattacharya, 1984); NP 82 (Newton and Perkins, 1982). For clarity, the T values from the thermometric formulation of Lee and Ganguly (1988) are not shown. Temperatures retrieved from core compositions are shown by filled symbols; open symbols are for temperature retrieved from rim compositions. The solidus for hydrous melting of granite and the aluminosilicate phase diagram is shown for reference only.

Fe)$_2$Al$_4$Si$_5$O$_{18}$ + 2KAlSi$_3$O$_8$ + 2H$_2$O], and not by the garnet decomposition reaction 2(Mg, Fe)$_3$Al$_2$Si$_3$O$_{12}$ + 4Al$_2$SiO$_5$ + 5SiO$_2$ → 3(Mg, Fe)$_2$Al$_4$Si$_5$O$_{18}$ + 2KAlSi$_3$O$_8$ + 2H$_2$O, since cordierite did not form at the expense of garnet.

5. P–T-deformation history of the supracrustal rocks in the Rengali orogen

5.1. Structural set-up

The prominent fabric in the Rengali schist belt is a crenulation cleavage, S$_{2SS}$. The schistosity in the ultramafic schists is defined by aggregates of antigorite (X$_{Mg}$ = 0.80–0.82) and tremolite (X$_{Mg}$ = 0.82–0.90); anthophyllite (X$_{Mg}$ = 0.69–0.70) occurs in modally subordinate amounts (Fig. 7a; analytical data in Supplementary Material 4), and albite and titanite occur as accessory phases. In the muscovite-

schists, the S$_{2SS}$ fabric is defined by defined by mica (muscovite ≫ biotite)-rich and quartz-rich layers (Fig. 8a) that wrap around garnet and staurolite porphyroblasts. In the schists, the earlier schistosity (S$_{1SS}$) is preserved as rootless folds (Fig. 8a) in domains interfolial to the S$_{2SS}$ layering, and as inclusion trails of quartz, ilmenite (rarely chlorite) in pre-D$_{2SS}$ garnet and staurolite porphyroblasts (Fig. 7b, c). In muscovite-kyanite schists (Fig. 7d), both the S$_{1SS}$ and S$_{2SS}$ fabrics are defined by kaolinite and muscovite intergrown with sieve-textured kyanite, hematite and rare ilmenite (pyrophyllite is rare); but kaolinite/pyrophyllite is lacking in the weakly-developed S$_{3SS}$ fabric defined by kyanite-muscovite aggregates. Analytical data in mica schists in the Rengali supracrustal belt is provided in Supplementary Material 5.

In the supracrustal rocks, the poles to S$_{2SS}$ describe a great circle girdle (Fig. 5b), and the measured axes of the D$_{3SS}$ folds plunge at shallow to moderate angles towards WSW and ENE (Fig. 3g, 5b). The weakly-developed axial planar fabric corresponding to these non-cylindrical
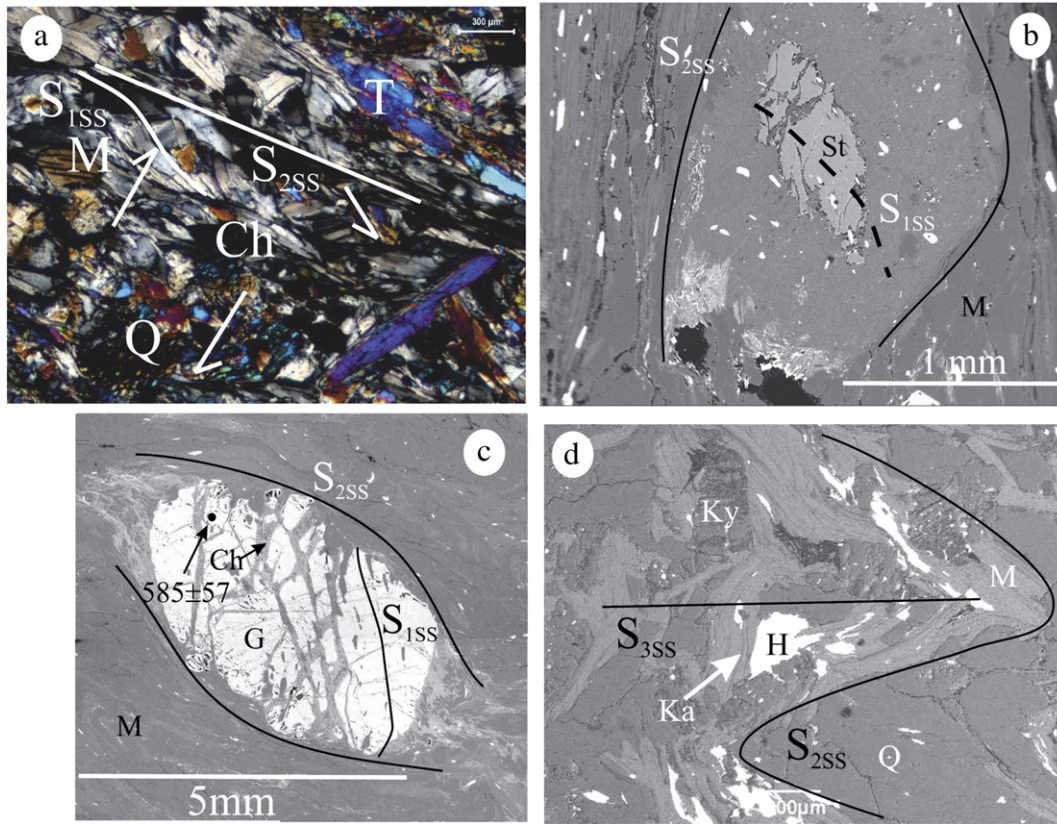
Fig. 7. Textural relations in the Rengali supracrustal belt. (a) XPL image of relict sigmoid S_{1SS} schistosity defined by shape preferred alignment of clinochlore in S_{2SS} interfolial domains defined by clinochlore and tremolite in ultramafic schist. (b) BSE image of a resorbed pre-S_{2SS} staurolite porphyroblast mantled by shimmer aggregates of randomly-oriented muscovite and chlorite in mica schist (PH-9B). Trails of S_{1SSS} schistosity (broken line) defined by ilmenite passes uninterrupted from within the resorbed staurolite to the fine-grained chlorite-muscovite aggregates. (c) BSE image (PH-9B) showing S_{1SS} inclusion trails defined by quartz lentils in garnet porphyroblast warped by S_{2SS} muscovite and quartz. Chlorite occurs along cracks within garnet and in the strain shadow zone. The chemical spot age ($\pm 2\sigma$ error in Ma) in monazite grain (filled circle) enclosed within the garnet is indicated. (e) BSE image (PH-10) showing folded S_{2SS} schistosity defined by intergrown muscovite and kaolinite. Note quartz-studded kyanite porphyroblast overgrows the S_{2SS} schistosity. Acronyms: Antigorite (Ch), kaolinite (Ka), kyanite (Ky), garnet (G), hematite (H), ilmenite (I), muscovite (M), plagioclase (P), staurolite (St), tremolite (T) and quartz (Q).

and asymmetric F_{3SS} folds is WNW-trending and steep-dipping (Fig. 5c). In contrast to the point maximum described by the F_{3SS} fold axes in regional scale, the F_{2SS} fold axes lie on an ill-defined girdle oriented at high angle to the mean orientation of the S_{3SS} axial plane (Fig. 5d). In D_{3SS} low-strain domains, the S_{1SS}/S_{2SS} intersection lineations (D_{2SS} fold axis) are curved on unrolled S_{2SS} surfaces and lie at a high angle with the hinge line of the D_{3SS} folds.

5.2. P–T conditions

The P–T evolutionary history of the mica schists (analytical data in Supplementary Material 5) was retrieved using P–T pseudosection analyses of two closely-spaced samples near the Barkote Shear Zone in the north, e.g. PH-9B (muscovite–staurolite–garnet–chlorite–quartz–ilmenite) and PH-10 (kaolinite–kyanite–muscovite–quartz–hematite ± pyrophyllite). The bulk compositions (in wt.% oxides) of the high–Al pelites are compared below:

	SiO_2	TiO_2	Al_2O_3	FeO (t)	MnO	MgO	CaO	Na_2O	K_2O	P_2O_5	Total
PH-9B	56.32	0.98	25.32	4.28	0.07	0.44	0.05	0.57	6.28	0.05	94.33
PH-10	51.68	0.80	29.61	5.32	-	0.57	0.04	0.45	5.24	0.05	93.76

In PH-9B, garnet and staurolite occur as mutually-exclusive pre-S_{2SS} porphyroblasts (Fig. 8a). Chlorite, muscovite, ilmenite and quartz occur as inclusions within garnet (Fig. 7c), and the porphyroblasts are altered along margins and intra-granular fractures to fine-grained muscovite-

chlorite aggregates that are syn/post-tectonic (Fig. 7b, c) with respect to S_{2SS} (data in Supplementary Material 5). Staurolite porphyroblasts are chemically homogenous, e.g. X_{Fe} [= Fe/Fe + Mg] = ca. 0.90, but garnet porphyroblasts are compositionally zoned (Fig. 8b, c). In the garnet porphyroblasts, X_{Fe}^* [= Fe / (Fe + Mg + Ca + Mn)] increases from 0.84 in the core to 0.90 in the rim, the steepest increase occurs near retrograde chlorite at the garnet margin, while X_{Fe} [= Fe/Fe + Mg] decreases slightly at ca. 0.91 in the grain interior, but increases sharply to 0.94 at the garnet margin (Fig. 8c). X_{Ca} [= Ca/(Fe + Mg + Ca] and X_{Mn} [= Mn/(Fe + Mg + Ca + Mn)] in garnet are low, and decrease from 0.05 to 0.03 and 0.03 to 0.01 respectively from the core to the margin (Fig. 8c).

Using the whole rock composition data, a MnCKFMASH P–T pseuodsection was constructed for PH-9B with H_2O ($X_{H2O} = 1.0$) and quartz in excess (Fig. 8d). In the P–T pseudosection, X_{Fe} [= Fe/Fe + Mg], X_{Ca} and X_{Mn} isopleths in garnet and X_{Fe} [= Fe/Fe + Mg] in staurolite decrease with increasing P and T. Therefore, the core → rim zoning profile in the garnet interiors suggests an initial prograde P–T path (decreasing X_{Fe}, X_{Ca} and X_{Mn}) within the muscovite ($\pm$ biotite)–staurolite–garnet–quartz phase field, followed by cooling-loading in the retrograde sector in the direction of decreasing X_{Ca} and X_{Mn}, but increasing X_{Fe}. The variations result in a counterclockwise P–T path for evolution of the rock, with T_{max} at ca. 600 °C, in the pressure range 5–6 kbar (Fig. 8d).

In PH-10, the bulk rock composition can be approximated by the system KFMASH. FeO (total) contents in muscovite vary between 2.5 and 3.3 wt.%, and in kaolinite and kyanite are lower at 0.3–1.1 wt.% and 0.6 and 0.7 wt.% respectively (analytical data in Supplementary
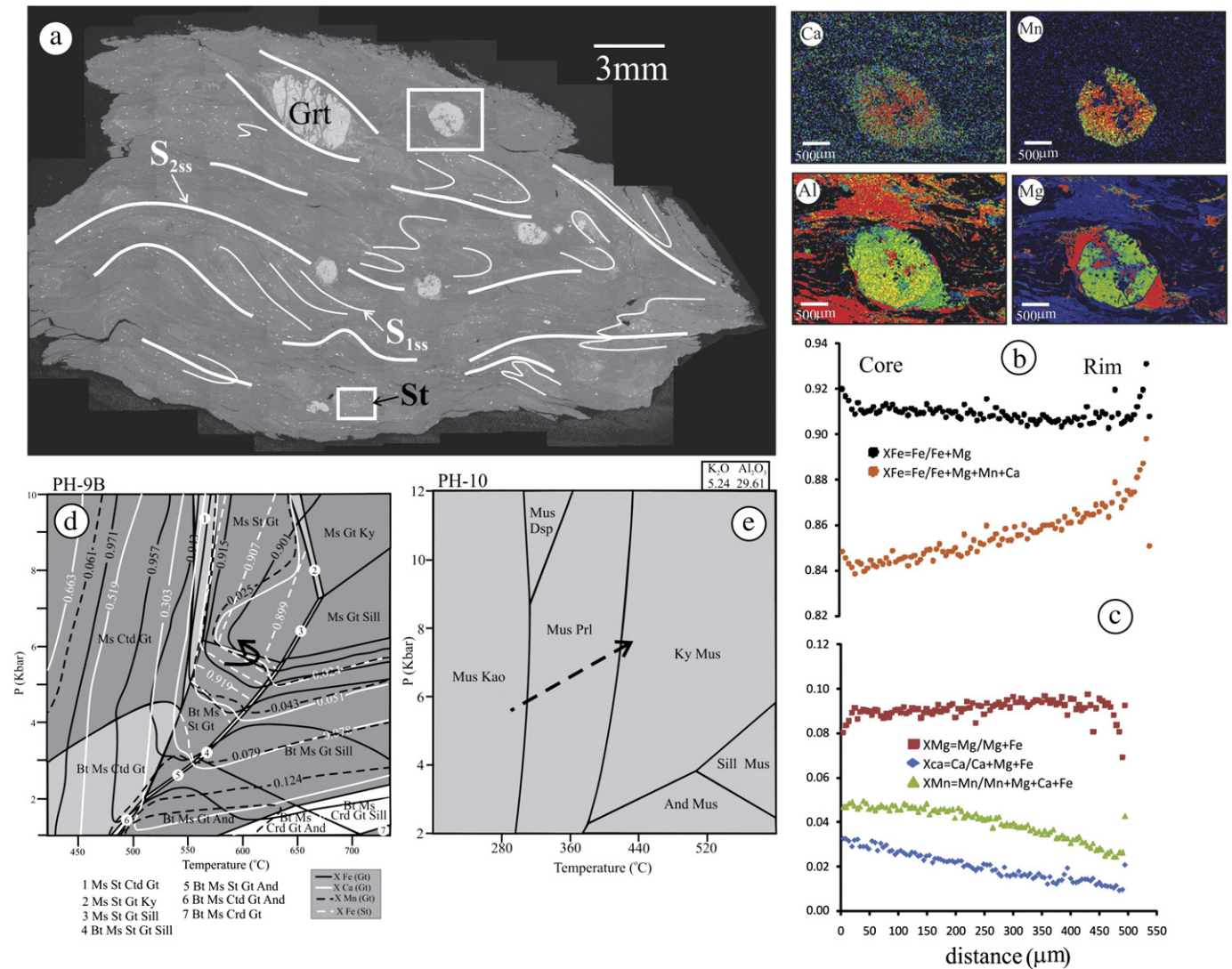
Fig. 8. (a) BSE image of thin section of PH-9B showing interfolial D$_{2SS}$ folds on S$_{1SS}$ schistosity. The box shows the occurrence of garnet analyzed in (b) and (c). (b) Ca, Mn, Fe, Mg X-ray element maps of the pre-S$_{2SS}$ garnet porphyroblast, and (c) core to rim zoning profile in the garnet. (d, e) MnCKFMASH and KASH P–T pseudosections for PH-9B and PH-10 respectively showing the P–T evolutionary paths for the rocks. Bulk rock compositions for the rocks provided in text. Locations of PH-9B, 10 are in Appendix A.

Material 5). Therefore, the bulk of FeO in the rock is contained in the modally abundant hematite grains, and in ilmenite. Ignoring FeO and MgO, a KASH P–T pseudosection is constructed for the rock (Fig. 8d), with H$_2$O and quartz in excess. The phase relations suggest that the stabilization of post-S$_{2SS}$/syn-S$_{3SS}$ kyanite-muscovite at the expense of S$_{1SS}$/S$_{2SS}$ kaolinitie (pyrophyllite)–muscovite assemblage was promoted by prograde heating at sub-greenschist facies conditions, 280–360 °C at pressure < 8 kbar, in the absence of diaspore in the rock.

Chattopadhyay et al. (2015) reconstructed a single "clockwise" P–T path for the mica schists in the Rengali supracrustal belt extending from 2 kbar, <300 °C to 7 kbar, ~750 °C; the P–T path was constructed across model reactions in rocks of diverse bulk composition, and extrapolating a path across the P–T loci of these reactions in the KFMASH P–T grid of Spear and Cheney (1989), culminating at the high-P, T end with the results of mineral thermo-barometry. The reconstructed P–T path leads to several ambiguities, e.g. (a) chloritoid should be a stable phase in the supracrustal rocks, but the mineral is absent in the schists, (b) staurolite and/or garnet are absent in the kyanite–kaolinite–muscovite schists, and the converse is true for the garnet/staurolite bearing schists, and (c) at the high P–T end, the muscovite–quartz assemblage in the schists is likely to have decomposed to K-feldspar–sillimanite assemblages, even if hydrous conditions prevailed. Instead, the large

difference (>300 °C; Fig. 8d–e) in the peak-temperature in the chemically diverse rocks (PH-9B, 10) located proximally close to the northern fringe of the Rengali orogen suggest the different litho-tectonic domains within the supracrustal belt evolved along diverse metamorphic P–T paths depending on the local tectonic set-up. Subsequently, these disparately-evolved metamorphic units within the supracrustal belt were tectonically juxtaposed. The situation typically occurs in accretion zones where inter-leaved domains exhibit variable P–T evolutionary histories as these units are subducted to variable depths and subsequently exhumed (Selverstone, 1985; Selverstone et al., 1984; Spear, 1989). Apparently, the "clockwise" P–T loop of Chattopadhyay et al. (2015) is a locus of metamorphic P–T conditions attained at different time in rocks of diverse bulk compositions in the different accretionary domains.

6. P–T of deformation in granitoid in the Rengali orogen

Granitoids exhibit a single tectonic fabric (fabric definition after Paterson et al., 1989), equivalent to S$_{3Gn}$ in the anatectic gneisses. The fabric is weakly developed in the interior of the granitoids, but the strain intensifies to near-mylonitic at the pluton margin. Mesoscale S-C fabrics and asymmetry in feldspar clasts indicate dextral sense of shear. The

mylonitic foliation is defined by polycrystalline quartz ribbons with pronounced deformation bands and strain wavy extinction, and shape-preferred aggregates of biotite flakes, and epidote (Fig. 7a). Typically, the foliation warps around clasts of former magmatic plagioclase grains showing core–mantle structures or appear to be replaced by aggregates of polygonized feldspar. Grain bulging (280–400 °C), recrystallization by sub-grain rotation (450–500 °C; Stipp et al., 2002; Lee et al., 2012b), and core–mantle structures in feldspars (450–600 °C; Gapais, 1989; Tullis and Yund, 1991) suggest recrystallization by grain boundary migration was accommodated by sub-grain rotation during mylonitization at 500 and 600 °C. The paucity of myrmekite (Altenberger and Wilhelm, 2000; Olsen and Kohlstedt, 1985; Tullis and Yund, 1987), the lack of dynamic recrystallization in magmatic hornblende porphyroclasts (brittle → ductile transition at ca. 640 °C; Cao et al., 2007), and the absence of chess-board twinning in quartz (ca. 650 °C; Kruhl, 1996) suggest that 600 °C was possibly the maximum temperature attained during the D_{3Gn} mylonitization.

7. P–T conditions in the Kantilo shear zone, EGGB

The shear zone at Kantilo (80 km south of Angul) is a segment of the E-trending, N-dipping Mahanadi shear zone (Lisker and Fachmann, 2001; Mahapatro et al., 2009) arguably defining the southern boundary of the Grenvillian-age granulites of the Angul domain (Rickers et al., 2001). The extensional (Mahapatro et al., 2009) shear zone hosts intensely–deformed and mylonitized charnockite and enderbite gneisses, leptynites (definition after Mehnert, 1972), garnet-sillimanite gneisses, and garnetiferous mafic granulite (Mahapatro et al., 2009). Within the Kantilo shear zone (KSZ), the pre-shearing

high-T annealing recrystallization texture exhibited by broadly equant and strain-free aggregates of polygonized feldspar and ferromagnesian minerals (pyroxene and hornblende), with garnet anchored to the polygonized matrix, are replaced by "flaser-textured" arrangement among minerals, e.g. straight-walled quartz ribbons, linear aggregates of polygonized feldspar, and drawn out aggregates of fine-grained orthopyroxene-plagioclase aggregates that wrap around garnet porphyroblasts. The polygonized minerals in the mylonite fabric exhibit high-degree of internal strain and share high-energy grain/phase boundaries indicating poor annealing among minerals (Passchier and Trouw, 1998) post-dating shearing. The rims of the pre-mylonite garnet porphyroblasts commonly overgrow the mylonite foliation. P–T estimates were obtained for the compositions (analytical data in Supplementary Material 6) of garnet (rim) and orthopyroxene–plagioclase aggregates defining the mylonite fabric using the Opx–Grt–Pl–Qtz thermo-barometric formulations listed in Fig. 6. For KSZ-hosted enderbite mylonites, the formulations yield the P–T values, 5–7 kbar and 750–950 °C. The estimated temperature for the KSZ is consistent with the occurrence of dynamically recrystallized orthopyroxene (T ≥ 750 °C; Cannat and Casey, 1995) in the mylonite fabric.

8. Age determinations

Results of U–Th–Pb (total) monazite age determinations made on 656 spots in 21 samples from different litho-tectonic domains within and bordering the Rengali orogen are presented in Figs. 9, 10. Electron probe microanalyses and age data of monazites are provided in the Supplementary Material 7a, b. SIMS U–Pb and Pb–Pb zircon ages (Figs. 11, 12) were determined (Table 1) in the anatectic biotite-
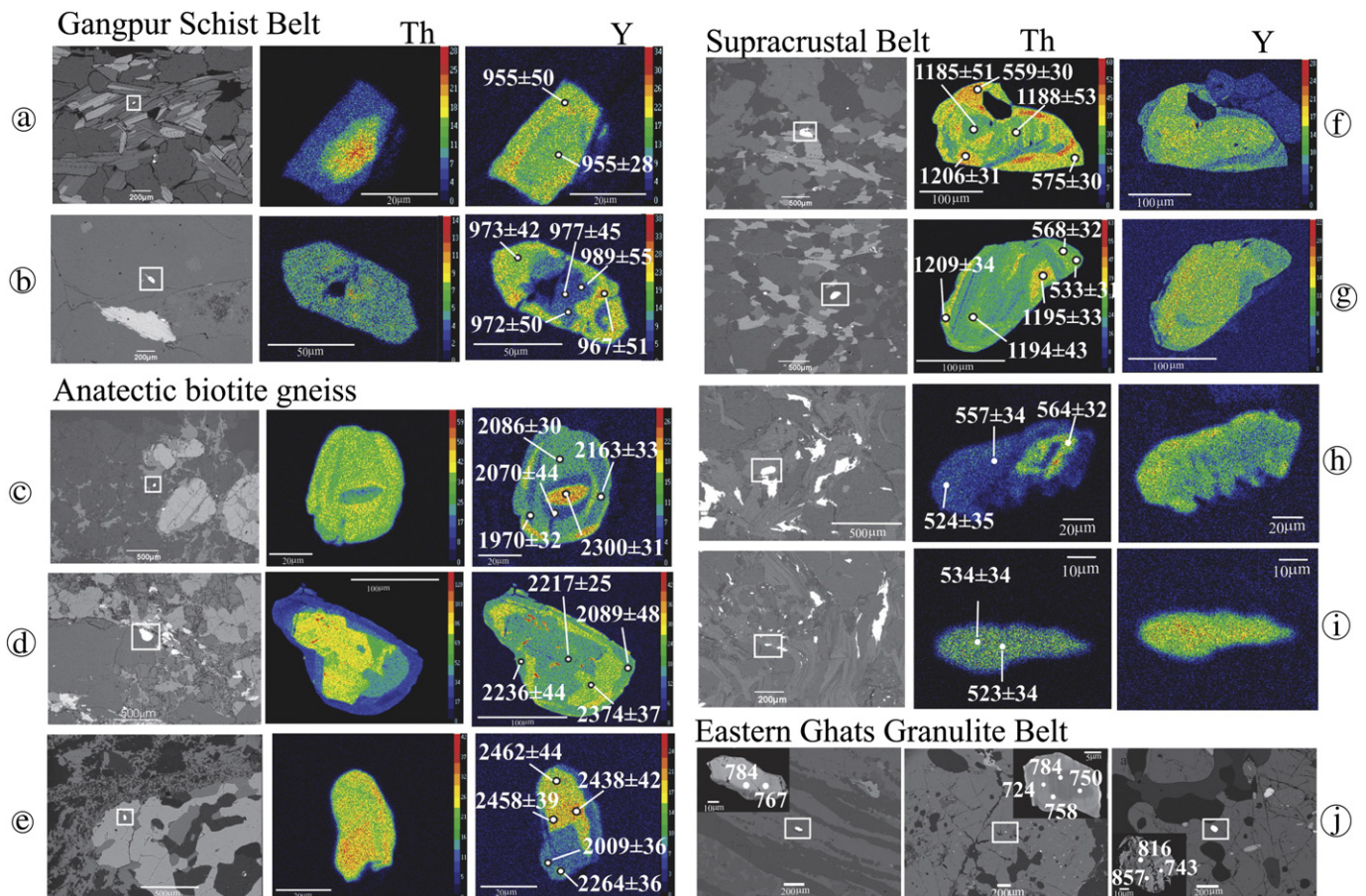
Fig. 9. Textural relations (BSE images), and Th and Y variations in monazites in (a, b) Gangpur Schist Belt, (c–e) anatectic garnet-biotite gneiss, (f–i) mica schists in the Rengali supracrustal belt, and (j) sheared leptynite and charnockite in the Kantilo shear zone, EGGB. In "j" chemical variations in monazite in insets in the three images are keyed to BSE images.
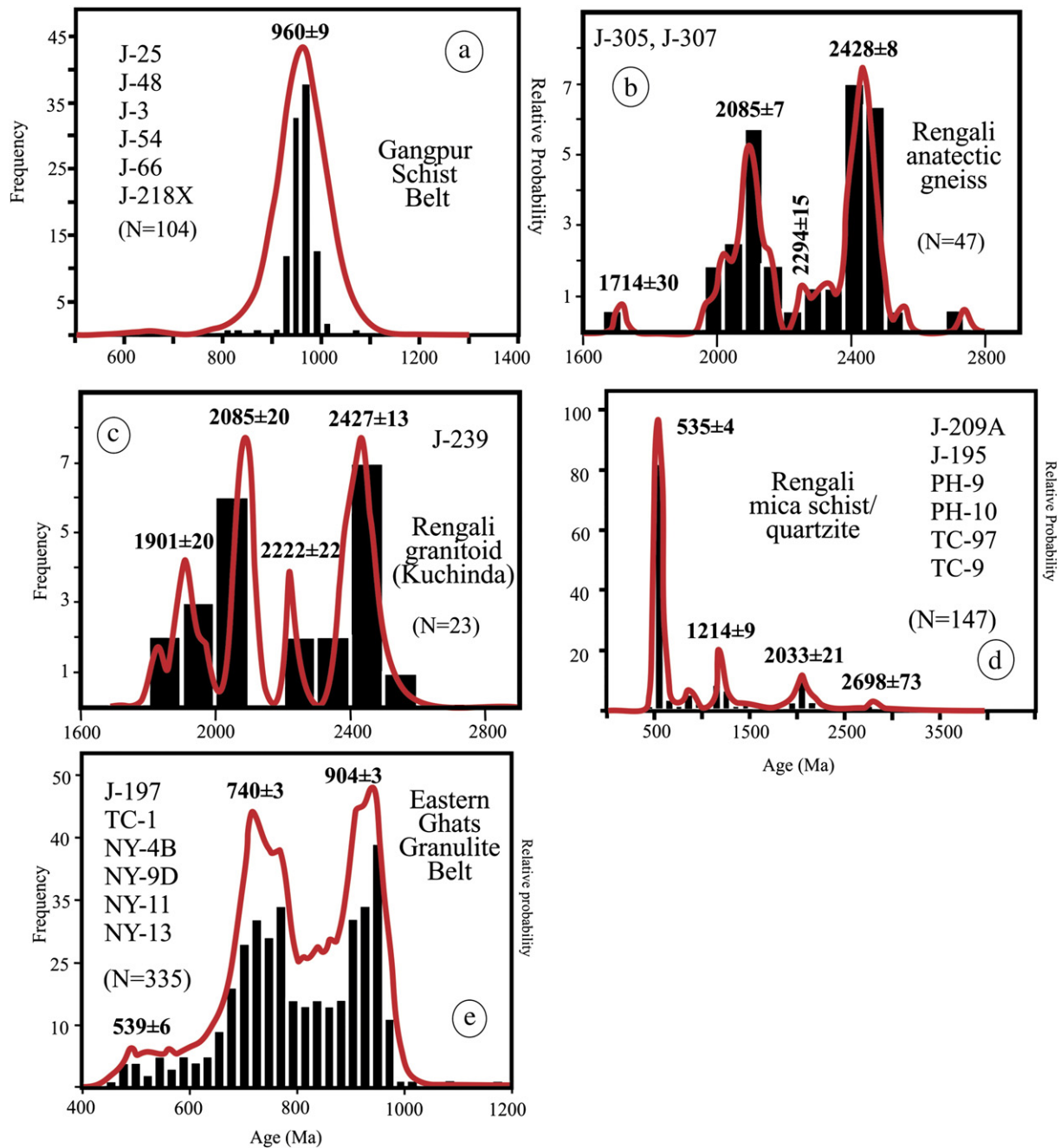
Fig. 10. Probability density plots of chemical ages obtained in monazites in (a) the Gangpur Schist Belt, (b) anatectic garnet-biotite gneiss, (c) Kuchinda granitoid, (d) mica schist/quartzite in the Rengali supracrustal belt, and (d) Eastern Ghats Granulite Belt. N = total number of spot ages; sample numbers in each lithodemic unit indicated. Statistically-resolved mean of age populations in the samples, and the locations of samples are indicated in Fig. 9.

garnet gneisses (J-307, 309, 180A) and in the Kuchinda granitoid (J-240). The locations of rocks used for monazite and zircon age determinations are shown in Fig. 13. The analytical conditions, the data reduction procedures, and the accuracy and precision of the age determinations in monazite and zircon are summarized in Appendices C and D respectively.

8.1. Monazite age determinations

8.1.1. Gangpur Schist Belt

Subhedral to euhedral monazites in mica schists (Fig. 9a, b) are commonly lineated parallel to the penetrative S_{2GS} schistosity or overgrow the fabric (Fig. 9b). These metamorphic monazites are typically zoned, with anhedral cores mantled by Th-poorer and Y-richer rims (Fig. 9a,

b). U and Pb variations across the chemically distinct domains are weak or lacking. In the sheared granitoids north of the GSB (Fig. 2), monazites occur within, and at grain/phase boundaries of, polygonized aggregates that replace former quartz and feldspar porphyries. Monazites in these variably deformed granitoids are also zoned, albeit with Th-poorer, Y-richer cores relative to the rims. However, regardless of the textural settings and the nature of zoning in monazite, 100 spots ages in 6 samples of granitoids and Gangpur schists yield chemical ages between 911 ± 40 Ma and 1014 ± 90 Ma, with a single spot age at 1061 ± 62 Ma (Fig. 10a; Supplementary Material 7), and the three spot ages between 825 ± 46 Ma and 646 ± 38 Ma (Fig. 10a; Supplementary Material 7). Barring the set of 3 younger ages and the oldest age detremination, the age range is similar to the monazite chemical ages obtained for a foliated granite (G7; 913 ± 30 Ma to 1034 ±
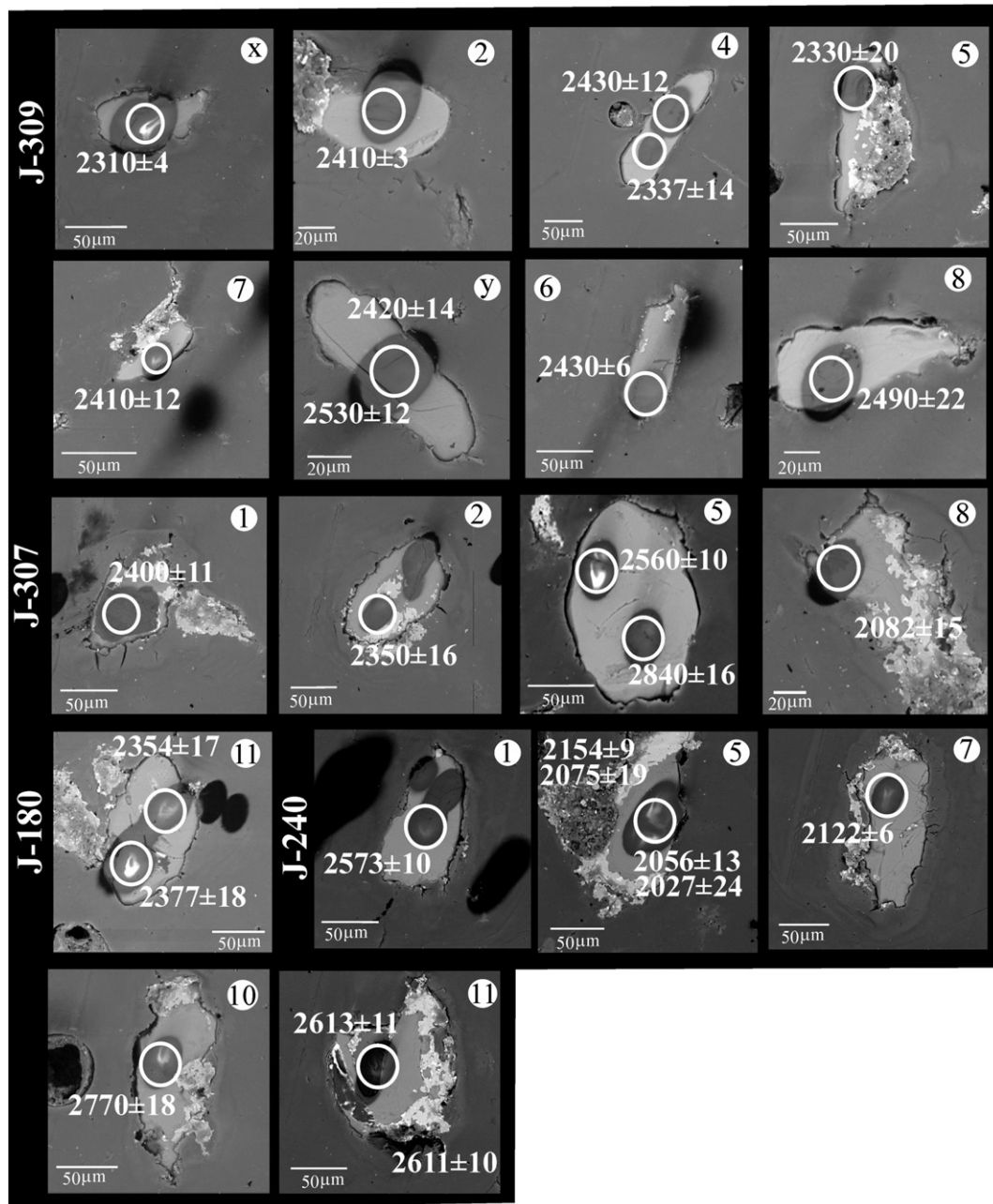
Fig. 11. Representative BSE images showing shape and structure of the analyzed zircon grains. $^{207}Pb/^{206}Pb$ spot ages with 1σ errors (Table 1) are shown. Circled letters/numbers identify the spots that occur as superscript appended to the sample numbers in Table 1.

31 Ma; 38 spot ages) and a massive granite (G9; 900 ± 30 Ma to 1040 ± 51 Ma; 25 spot ages) in Sargipalli (SW of Sundergarh, Fig. 2) hosted within GSB schists (Chowdhury and Lentz, 2011). For the 2σ errors in monazite chemical ages (Supplementary Material 7), no age difference could be resolved between the core and rim in the individual monazite grains, as well as for monazites within granitoids and schists. Accordingly, the mean age of deformation–metamorphism in the Gangpur Schist Belt was taken to be 960 ± 9 Ma (Fig. 10a). The Grenvillian-age for the growth of metamorphic monazites is pervasive throughout the belt, barring domains adjacent to the Singhbhum craton that were not sampled (Fig. 13).

8.1.2. Anatectic biotite-garnet gneisses and the Kuchinda granitoid, Rengali orogen

Monazites were analyzed in two anatectic garnet–biotite gneisses (J-305 and J-307; 47 spot ages; Fig. 9c–e, 10b; Supplementary Material

7), and in the structurally younger (post-S$_{2Gn}$/pre-S$_{3Gn}$) Kuchinda granitoid (J-239; 23 spot ages, Fig. 10c; Supplementary Material 7). Monazites in the anatectic orthgneisses are rare, skeletal and patchy, and Th, U and Pb abundances in these monazites are too low for robust and reproducible chemical age determinations. Hence, monazite chemical age data in the gneisses are not reported.

Monazites in the gneisses are profuse, commonly 50–100 μm long (up to 300 μm), typically subhedral to anhedral in shape, and complexly zoned in Th and Y (Fig. 9c–e); U and Pb zoning is weak or lacking. The monazites within the melanocratic layers in garnet-biotite gneisses typically exhibit three distinct polychronous chemical domains (Fig. 9c–e). The innermost, xenomorphic cores in the monazites yielded the oldest ages between 2400 and 2500 Ma (mean age 2428 ± 8 Ma); at least one Neoarchean spot age with low 2σ error (2737 ± 37 Ma) was obtained in a xenomorphic core in J-307 (Fig. 10b). The cores are mantled by chemically-homogeneous annular rims; the chemical ages of these
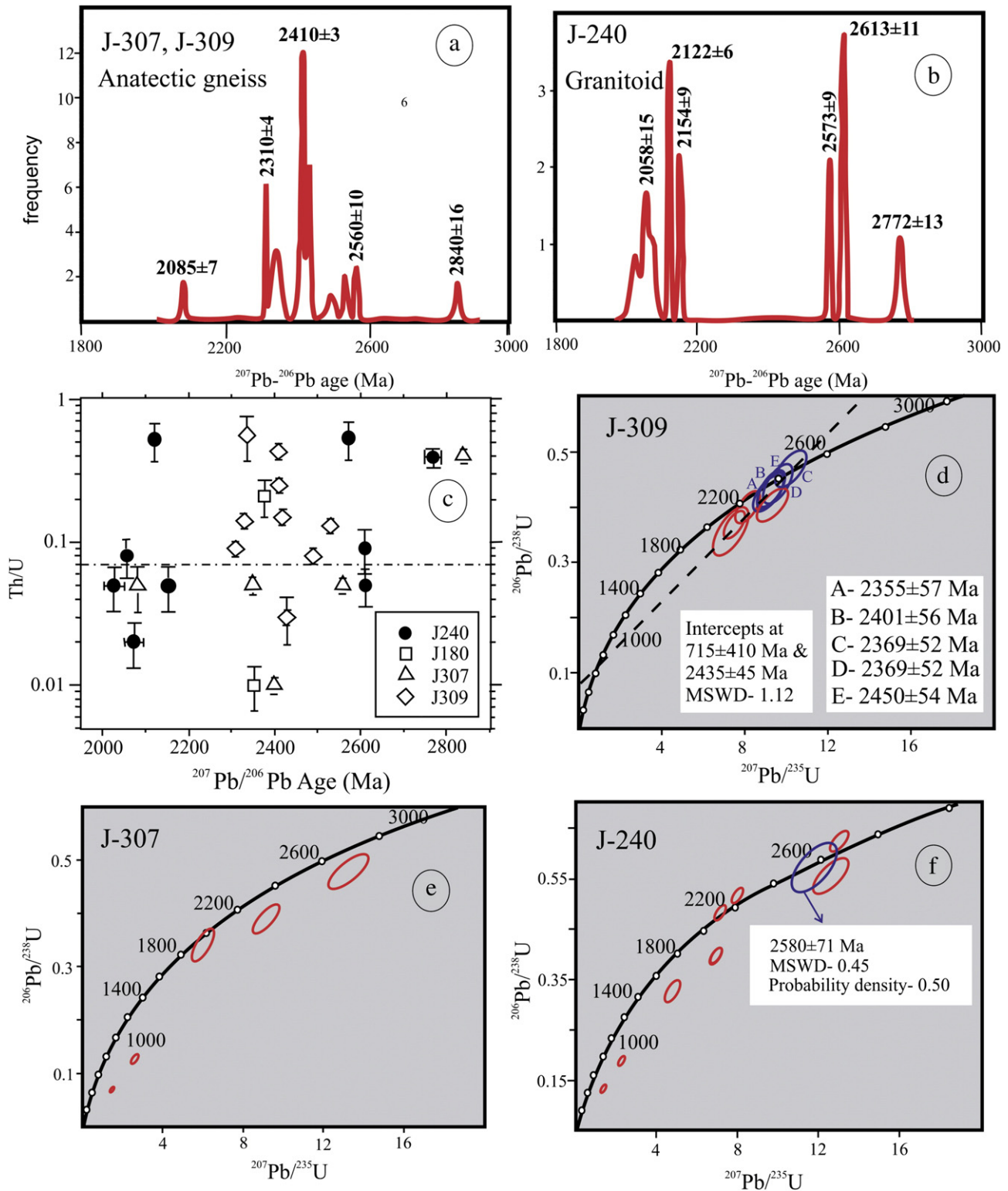
Fig. 12. Frequency diagrams of Pb–Pb zircon ages in anatectic gneisses (a) and the Kuchinda granitoid (b); (c) ^{207}Pb–^{206}Pb vs. Th/U plot of analyzed zircons in anatectic gneisses and the granitoid after Hoskin and Schaltegger (2003); U–Pb concordia diagrams for garnet-biotite anatectic gneisses (d–e) and the Kuchinda granitoid (f). Data in Table 1. In (d), A to E are near-concordia ages.

rims lie between 2200 Ma and 2350 Ma (mean age 2294 ± 15 Ma). The outermost rims yield the youngest ages; an overwhelming number of these ages are tightly constrained between 1950 Ma and 2100 Ma (mean age 2085 ± 7 Ma). In leucosome-hosted monazites, the Neoarchean ages are lacking, the frequency of oldest Paleoproterozoic ages is uncommon, but the two younger Paleoproterozoic age

populations with mean ages of 2317 ± 14 Ma and 2064 ± 14 Ma are common. Some of the unusually large monazites in leucosomes are chemically homogenous, and these monazites yield tightly-constrained ages (2000–2100 Ma), identical to the youngest Paleoproterozoic rims (2064 ± 14 Ma) in the matrix monazites. In the Kuchinda granitoid, the Early Neoarchean age population is lacking,

Table 1
SIMS U–Pb isotope data and ages measured in zircon in the Rengali anatectic gneisses and the deformed Kuchinda granitoid.

Sample no	U (ppm)	1 s.d.	Th (ppm)	1 s.d.	Th/U	Radiogenic isotopic ratios				Correlation coefficient	Apparent Ages (Ma) ± 1 s.e						% radiogenic ^{206}Pb
						$^{207}Pb/^{235}U$	1 s.e.	$^{206}Pb/^{238}U$	1 s.e.		$^{207}Pb/^{235}U$	1 s.e.	$^{206}Pb/^{238}U$	1 s.e.	$^{207}Pb/^{206}b$	1 s.e.	
J 240[1]	407	70	216	52	0.53	1.47E + 01	5.85E-01	6.19E-01	2.53E-02	0.99	2793	38	3107	101	2573	9	98.79
J-240[5]	543	94	43	10	0.08	6.98E + 00	2.11E-01	3.99E-01	1.21E-02	0.97	2109	27	2164	56	2056	13	98.73
J-240[5]	4189	906	228	61	0.05	1.26E + 00	8.66E-02	7.32E-02	4.95E-03	0.98	829	39	456	30	2027	24	92.12
J-240[5]	3495	756	58	16	0.02	2.19E + 00	1.40E-01	1.24E-01	7.77E-03	0.99	1176	45	751	45	2075	19	95.69
J-240[5]	2188	473	119	32	0.05	4.69E + 00	3.10E-01	2.53E-01	1.67E-02	1.00	1765	55	1455	86	2154	9	97.38
J 240[7]	87	15	45	11	0.52	7.82E + 00	2.33E-01	4.30E-01	1.28E-02	0.99	2210	27	2307	58	2122	6	99.88
J 240[10]	722	58	280	36	0.39	1.25E + 01	7.25E-01	4.67E-01	2.60E-02	0.98	2640	55	2470	114	2770	18	99.77
J 240[11]	1557	268	71	17	0.05	1.29E + 01	3.76E-01	5.31E-01	1.62E-02	0.98	2670	28	2745	68	2613	11	99.32
J-240[11]	677	146	62	17	0.09	1.16E + 01	9.02E-01	4.81E-01	3.72E-02	1.00	2576	72	2532	162	2611	10	99.05
J 180A[11]	1064	183	223	54	0.21	8.02E + 00	3.39E-01	3.81E-01	1.51E-02	0.97	2233	38	2081	70	2377	18	99.35
J-180A[11]	1528	330	17	5	0.01	8.48E + 00	6.85E-01	4.08E-01	3.32E-02	0.99	2283	73	2205	152	2354	17	99.45
J 307[1]	6058	394	74	8	0.01	1.48E + 00	7.58E-02	6.93E-02	3.59E-03	0.99	921	31	432	22	2400	11	96.22
J 307[2]	3498	245	167	21	0.05	2.62E + 00	1.46E-01	1.27E-01	7.32E-03	0.99	1310	41	770	42	2350	16	94.26
J 307[5]	1660	109	80	8	0.05	9.15E + 00	5.03E-01	3.89E-01	2.11E-02	0.99	2350	50	2120	98	2560	10	99.31
J 307[5]	436	28	173	18	0.40	1.32E + 01	7.65E-01	4.77E-01	2.70E-02	0.99	2700	55	2510	118	2840	16	99.83
J-307[8]	953	206	50	13	0.05	6.01E + 00	4.45E-01	3.38E-01	2.41E-02	0.99	1977	65	1879	116	2082	15	99.59
J 309[X]	1444	102	124	13	0.09	8.10E + 00	4.72E-01	4.00E-01	2.32E-02	1.00	2240	53	2170	107	2310	4	99.75
J 309[2]	1163	75	505	52	0.43	9.11E + 00	5.80E-01	4.24E-01	2.71E-02	1.00	2350	58	2280	123	2410	3	99.84
J 309[4]	1859	121	47	17	0.03	9.60E + 00	5.99E-01	4.42E-01	2.91E-02	1.00	2400	57	2360	130	2430	12	99.76
J-309[4]	266	58	149	40	0.56	7.32E + 00	7.24E-01	3.56E-01	3.55E-02	1.00	2152	88	1962	169	2337	14	98.89
J 309[5]	1320	86	182	19	0.14	7.49E + 00	4.30E-01	3.67E-01	2.04E-02	0.98	2170	51	2010	96	2330	20	99.41
J 309[7]	885	57	219	22	0.25	9.26E + 00	5.31E-01	4.31E-01	2.54E-02	0.99	2360	53	2310	114	2410	12	99.84
J 309[Y]	1438	94	192	20	0.13	9.32E + 00	6.13E-01	4.05E-01	2.64E-02	0.99	2370	60	2190	121	2530	12	99.86
J 309[Y]	1329	86	198	21	0.15	9.25E + 00	5.44E-01	4.28E-01	2.49E-02	0.99	2360	54	2300	112	2420	14	99.89
J 309[6]	2540	164	87	9	0.03	1.02E + 01	6.01E-01	4.70E-01	2.75E-02	1.00	2460	54	2480	121	2430	6	99.96
J 309[8]	2117	143	177	20	0.08	1.38E + 01	8.98E-01	6.13E-01	3.71E-02	0.98	2740	62	3080	148	2490	22	97.52
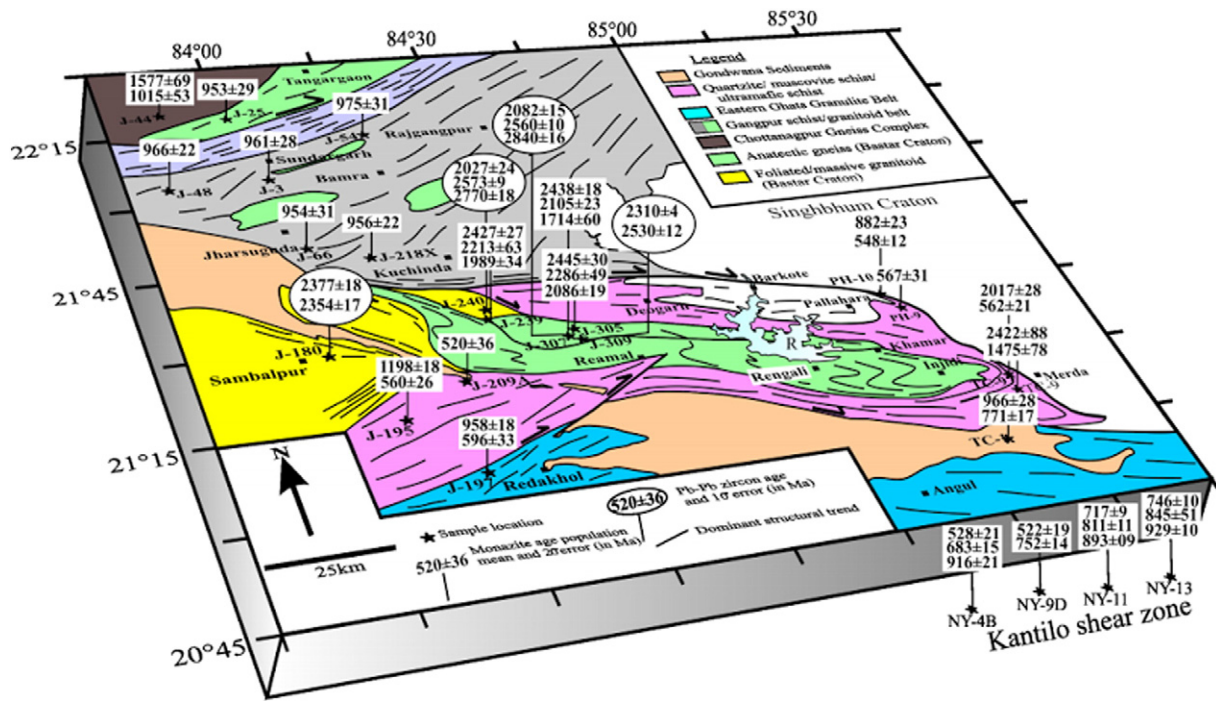
Fig. 13. Spatial distribution of monazite chemical ages (in boxes) and Pb–Pb zircon ages (in ellipses) in the Rengali orogen and its environ (this study). Locations of monazite-dated samples from the Kantilo area, barring NY-9D which has the same co-ordinates as NY-A, B in Appendix A: NY-4B [20°23.15′N, 85°01.04′E], NY-11 [20°22.55′N, 85°06.95′E] and NY-13 [20°22.50′N, 85°02.11′E].

but the textural relations and polychronous nature of the chemical domains are similar to the younger age populations in the anatectic gneisses. The gamut of Late Neoarchean and Paleoproterozoic chemical spot age data in the three rocks taken together can be statistically resolved into four age populations, with mean ages at 2427 ± 13 Ma, 2222 ± 22 Ma, 2085 ± 20 Ma and 1901 ± 20 Ma (Fig. 10c).

In the melanocratic layers in gneisses, monazites with the youngest Paleoproterozoic rims (2.1–1.9 Ga) overgrow the biotite-defined S_{1Gn}/S_{2Gn} fabrics. But these youngest Paleoproterozoic rims are lacking in monazites hosted within garnet porphyroblasts, barring one exception. In J-307, a monazite with 2.1 Ga rim occurs in a polymineralic aggregate included within garnet; but closer examination reveals that a fracture extends from the edge of the garnet grain to the polymineralic inclusion. This may suggest that the growth of 2.1–1.9 Ga monazites may have been induced by fluid-induced precipitation. If so, the unusually-large and chemically-homogeneous ca. 2.1 Ga monazite in the leucosome, albeit in contact with rafts of melanocratic matrix stranded with the leucosome, was similarly produced. The textural evidence taken together suggest that growth of garnet, at least parts of it, are younger than 2.4–2.3 Ga, i.e. the pre/syn-D_{1Gn} anatexis in the gneisses was synchronous with 2.4–2.3 Ga, and the younger (S_{2Gn}) tectonic fabric pre-dated 2.1–1.9 Ga. It appears therefore that pre/syn-D_{1Gn} melting and high-grade metamorphism and deformation (D_{1Gn} and S_{2Gn}) in the anatectic garnet-biotite gneisses occurred during the Early Paleoproterozoic, 2.5–2.4 Ga. The older (Neoarchean) age possibly correspond to the age of inherited monazite grains.

8.1.3. The Rengali Supracrustal Belt

Monazites in mica schists and micaceous quartzites in the belt are texturally complex (Fig. 9f–i). The monazites can be grouped in two broad textural types, e.g. (a) anhedral and circular-shaped monazites typically pre-tectonic with respect to the prominent S_{2SS} schistosity (Fig. 9f, g), and included within pre-S_{2SS} garnet and staurolite porphyroblasts, and (b) euhedral and inclusion-free metamorphic monazites lineated parallel to the S_{2SS} schistosity and along axial planes of D_{3SS} folds (Fig. 9h, i). 'Type a' monazite grain interiors are complexly

zoned; these monazite cores yield a wide age range, with mean age populations at 2698 ± 73 Ma, 2033 ± 21 Ma, 1214 ± 9 Ma and 867 ± 21 Ma (Fig. 10d). Different samples yield different core ages. However, the thin rims mantling older cores in the 'type a' monazites in the matrix are invariably Pan African in age (505–610 Ma). These monazites rims often truncate chemical zones in the older cores, and therefore, these Pan African metamorphic rims are inferred to have precipitated by fluid-aided dissolution-precipitation (Rasmussen and Muhling, 2007; Rasmussen et al., 2005; Rekha and Bhattacharya, 2014). We suggest that the lack of Pan African rims in monazites included within the porphyroblasts is because these monazites were shielded from fluid access, and hence did not precipitate the Pan African rims (cf. Rekha and Bhattacharya, 2014). By contrast, 'type b' chemically-homogeneous metamorphic monazites yield ages between 505 ± 10 Ma and 610 ± 15 Ma, with the mean age population at 535 ± 4 Ma (Fig. 10d). Of the total number of 151 spot ages determined in seven mica schist/micaceous quartzites in the Rengali orogen, ~60% of the chemical ages are Pan African. The ages of 'type b' metamorphic monazite are identical to the SHRIMP U–Pb (zircon) ages (511–552 Ma) obtained in the nepheline syenite gneisses at Khariar (Fig. 1) emplaced synchronous with the westward thrusting of the EGGB over the Bastar Craton (Biswal et al., 2007).

8.1.4. Eastern Ghats Granulite Belt-northern fringe

Chemical ages in monazites (Fig. 9j) in garnet-sillimanite gneiss, leptynite and foliated enderbite-charnockite in the high grade belt, taken together, yield three statistically-resolved age populations, e.g. 925 ± 7 Ma, 740 ± 3 Ma and 539 ± 12 Ma (Fig. 10d). The Early Neoproterozoic and Pan African ages are widely reported from the Neoproterozoic domain within the EGGB (Aftallion et al., 1988; Krause et al., 2001; Mezger and Cosca, 1999); Pan African ages are also reported in the neighboring craton adjacent to the EGGB (Aftalion et al., 2000; Aftallion et al., 1988; Biswal et al., 2007; Upadhyay et al., 2006). The significant aspect of the age determinations in this study is the identification of the mid-Neoproterozoic age populations (Fig. 10d) in the KSZ mylonites. The mid-Neoproterozoic age populations are obtained from

monazites lineated parallel to (Fig. 9j, left) and overgrowing the granulite-facies mylonite fabric, and in monazites hosted within garnet that overgrow the KSZ fabric (Fig. 9j, middle and right). By contrast, the Pan African monazites in the KSZ occur exclusively in the fine-grained-mineral mosaic in the mylonites, and not within the garnet porphyroblasts. Since the mid-Neoproterozoic monazites occur both in the mylonite fabric as well as in garnet mantles overgrowing the fabric, we suggest that the high–T deformation in the Kantilo shear zone is mid-Neoproterozoic in age.

The range of mid-Neoproterozoic metamorphic ages overlaps with similar ages reported in areas fringing the northern and western margins of the EGGB. For example, Krause et al. (2001) report concordant U–Pb age (792 ± 2 Ma) obtained in abraded zircon grains that exhibit igneous interiors mantled by metamorphic rims in ferrodiorites from the Chilka Lake anorthosite. Dobmeier and Simmat (2002) relate the mid-Neoproterozoic monazite chemical ages in the Chilka Lake to cooling of the aureole around the Chilka Lake anorthosite pluton (762–743 Ma) followed by fabric-forming transpressional deformation (690–662 Ma). Hippe et al. (2015) retrieved concordant U–Pb zircon ages between 869 ± 7 Ma and 690 ± 1 Ma in the nepheline syenite complex at Koraput close to the western margin of the EGGB. The authors suggest the oldest age corresponds with the emplacement of the Koraput alkaline complex, whereas the younger (<860 Ma) ages relate to episodic partial resetting of the U–Pb ages induced by recrystallization. The youngest U–Pb ages (700–690 Ma) reflect a final pulse of high-grade metamorphism in the Koraput area (Hippe et al., 2015).

8.2. Zircon age determinations in anatectic gneisses and the Kuchinda granitoid

Zircon grains in the garnet-biotite anatectic gneisses (J-307, J-309), and a hornblende gneiss (J-180A) occurring as enclave within the Sambalpur granitoid, show weak cathodoluminescence response. In BSE images (Fig. 11), the fully-exposed grains are weakly zoned. The ^{207}Pb–^{206}Pb ages in the anatectic garnet-biotite gneisses J-307, 309 show four prominent age probability peaks at 2840 ± 16 Ma, 2560 ± 10 Ma, 2410 ± 3 Ma and 2310 ± 04 Ma, and a subsidiary age population with mean peak age at 2085 ± 7 Ma (Fig. 12a). Two Pb–Pb ages in J-180 are 2377 ± 18 and 2354 ± 17 Ma (Table 1). The ^{207}Pb–^{206}Pb ages in the Kuchinda granitoid (J-240) comprise three different age populations, e.g. Neoarchean age population at 2772 ± 13 Ma, 2613 ± 11 Ma, 2573 ± 09 Ma, and Paleoproterozoic age populations at 2154 ± 09 Ma, 2122 ± 13 Ma and 2058 ± 15 Ma (Fig. 12b). The range of Th/U values in 2.8–2.0 Ga zircons in the anatectic gneisses and the granitoid (Fig. 12c) suggests the zircons were originally magmatic (≥0.07) to likely metamorphic (~0.01) (Hoskin and Schaltegger, 2003).

The ^{207}Pb–^{235}U–^{206}Pb–^{238}U ages in the four samples are discordant (Fig. 12d–f). In the garnet-biotite anatectic gneiss J-309, the near-concordant ages (±2σ) computed using "unmix age' function (Isoplot: Ludwig, 2012) are 2355 ± 57 Ma (MSWD = 2.0, probability = 0.15), 2401 ± 56 Ma (MSWD = 0.50, probability = 0.48), 2369 ± 52 Ma (MSWD = 1.4, probability = 0.24), 2369 ± 52 Ma (MSWD = 2.2, probability = 0.14) and 2450 ± 54 Ma (MSWD = 0.38, probability = 0.54) (Fig. 12c). In the gneisses, the near-concordant U–Pb ages (Fig. 12d) are in good agreement with the two Pb–Pb probability peaks at 2410 ± 03 Ma and 2310 ± 04 Ma (Fig. 12a). In the granitoid sample J-240, the U–Pb age at 2580 ± 71 Ma (MSWD = 0.45, probability = 0.50) (Fig. 12f) is in good agreement with the Pb–Pb age at 2573 ± 09 Ma (Fig. 12b).

In the anatectic gneisses, U–Pb ages, the bulk of ^{207}Pb–^{206}Pb ages in zircons, and the monazite chemical ages, define an age range of 2.5–2.3 Ga that corresponds with pre/syn-D$_{1Gn}$ anatexis and high-grade metamorphism in the gneisses. The structurally younger post-D$_{2Gn}$ granitoids in the Rengali orogen are characterized by two ^{207}Pb–^{206}Pb zircon age populations, e.g. 2.6–2.5 Ga (one age of 2772 ± 13 Ma), and 2.2–2.0 Ga; the younger age population possibly

corresponds with the emplacement age of the Rengali granitoids. The ubiquitous 2.1–1.9 Ga rims in monazite in the gneisses and in the granitoids appear to have been precipitated by fluids released during granitoid emplacement. The older Neoarchean Pb–Pb ages (2.8–2.5 Ga) in granitoids possibly qualify as inherited ages.

9. Discussion

9.1. The Gangpur schists: westward extension the NSMB-CGC Grenvillian-age accretion zone?

In the Tebo–Kolomda sector (Fig. 1), located ca. 150 km ENE of Sundergarh and along the strike extension of the Gangpur Schist Belt, Mahato et al. (2008) established that the North Singhbhum Mobile Belt (NSMB), sandwiched between the Chottanagpur Gneiss Complex (CGC) in the north and the Singhbhum Craton in the south (Fig. 1), comprised two disparately-evolved longitudinal domains. The metamorphic age of the southern domain fringing the northern margin of the Singhbhum Craton is Mesoproterozoic, 1.5–1.7 Ga (Mahato et al., 2008). By contrast, metamorphism in the northern NSMB domain (north of the Dalma Ophiolite Belt; Fig. 1) is Grenvillian in age and fringes the southern margin of the CGC characterized by Mesoproterozoic (ca. 1.5 Ga) high-grade metamorphism overprinted by Grenvillian-age amphibolite-granulite facies metamorphism and granitoid emplacement (Maji et al., 2008; Rekha et al., 2011). The CGC and the NSMB northern domain share a highly tectonized Grenvillian-age contact (Rekha et al., 2011) that exhibits E–W trending non-cylindrical gently-plunging folds, a steeply-dipping south-vergent mylonite zone with gently-plunging stretching lineation, with reverse-dextral sense of movement on the fault plane. The northward transport of the NSMB over the CGC was associated with prograde amphibolite facies metamorphism and resulted in the stabilization of garnet and staurolite in the NSMB schists. Rekha et al. (2011) argued based on monazite chemical ages and LA-ICPMS zircon ages that the Grenvillian-age shear zone marked the closure of an ocean basin that culminated with the accretion of the CGC with the Singhbhum Craton.

In the Gangpur Schist Belt, the prograde P–T path reconstructed in the garnet-staurolite schist (Fig. 4), the Grenvillian age of the metamorphism in the schists (Fig. 10a), and the mesoscale deformation structures (Fig. 3), e.g. sub-horizontal stretching lineation in the ENE-trending mylonite zone and the non-cylindricity of gently-plunging folds with steep dipping axial planes are identical to the ones reported by Mahato et al. (2008) and Rekha et al. (2011) in the Tebo–Kolomda area. By implication, the Grenvillian-age accretion zone (Rekha et al., 2011) between the CGC and NSMB northern domain inferred in the Tebo–Kolomda (Fig. 1) appears to extend 150 km westward (Fig. 1). Since the ENE/NE-trending Grenvillian-age GSB fabric mantling the W/NW margins of the Singhbhum Craton is truncated and re-oriented parallel to the WNW-trending Rengali orogen (Fig. 2), the Rengali orogen is arguably younger relative to the Grenvillian age accretion (Rekha et al., 2011; this study).

9.2. The anatectic gneisses in the Rengali orogen: a septum of the Bastar Craton

The Paleoproterozoic chemical ages in monazites overlap favorably with Pb–Pb zircon ages and the U–Pb ages (Fig. 13) in the anatectic gneisses and the Kuchinda granitoid body. The age determinations together establish, for the first time, the existence of a high-grade gneiss domain affected by multiple Paleoproterozoic tectono-thermal events within the Rengali orogen. The hitherto uncharacterized domain exhibits four tectono-metamorphic events at ca. 2.7 Ga, 2.5–2.4 Ga, 2.3–2.2 Ga, and 2.1–2.0 Ga. The Neoarchean–Paleoproterozoic high-grade metamorphism–anatexis and the juvenile crust formation events have no known equivalents in the neighboring domains of the Neoproterozoic Eastern Ghats Granulite Belt (Aftallion et al., 1988;

Biswal, 2000; Biswal et al., 2007; this study), in the Grenvillian-age Gangpur Schist belt (this study), and in the older Paleo/Mesoarchean Singhbhum Craton in the north (Prabhakar and Bhattacharya, 2013, and references therein). Also, as the Paleoproterozoic domain is not restricted to the southern margin of the Singhbhum Craton, and becomes expansive and extends westward towards the Bastar Craton in the west, the Rengali gneisses cannot be explained by the southward growth of the Singhbhum Craton as suggested by Bose et al. (2013).

Instead the Paleoproterozoic ages can be easily reconciled with the gamut of ages available in the high-grade gneisses and felsic intrusive of the Bastar Craton in the west (Mohanty, 2015). For example, the 2.4–2.5 Ga age population in the anatectic gneiss can be correlated with similar ages obtained in various lithologies in the Bastar Craton, e.g. the Amgaon gneiss (U–Pb zircon age 2378 + 17, 2432 ± 5 Ma: Ahmad et al., 2009); Dongargarh granite (Rb–Sr whole-rock age, 2465 ± 22 Ma: Krishnamurthy et al., 1988); Malanjkhand gray gneiss (Rb–Sr whole-rock age, 2405 + 63: Panigrahi et al., 1993; Malanjkhand granite I (Rb–Sr whole-rock age, 2405 ± 63 Ma. 2467 ± 38: Panigrahi et al., 1993); Re–Os age, Stein et al., 2004: 2478 ± 9, 2477 ± 10; U–Pb zircon age, Panigrahi et al., 2002: 2490 ± 8 (A-28); Markampara granite (U–Pb zircon, Sarkar et al., 1993): 2480 ± 3; Katekalyan migmatite, Bengpal (Rb–Sr whole-rock age, 2530 ± 89 Ma; Bandyopadhyay et al., 1990).

The intermediate age cluster (2.3–2.2 Ga) correlates well with the age of granitoids bodies throughout the Bastar Craton, e.g. Paliam–Darba and Burugum granite (Rb–Sr whole-rock age, Pandey et al., 1989: 2275 ± 80, 2237 ± 70; Bijli rhyolite (Rb–Sr age, Sarkar et al., 1981: 2180 ± 25; Dongargarh granite phase II (Rb–Sr age, Sarkar et al., 1981; 2270 ± 90); Malanjkhand granite phase II (Rb–Sr whole-rock age, Panigrahi et al., 1993: 2243 ± 217; 2106 + 102). While the youngest age cluster (2.0–2.1 Ga) correlates well with those in the 2106 Ma Tirodi gneiss II (Sm–Nd age, Ahmad et al., 2009) and the 2095 ± 118 Ma Bastar granite (Rb–Sr whole-rock age, Sarkar and Gupta, 1990). Summarizing, we suggest that the Paleoproterozoic high-grade anatectic gneisses and granitoids in core of the Rengali orogen is a septum of the Bastar Craton caught up in a younger accretion event within the Rengali orogen.

9.3. The Rengali supracrustal belt: a Pan African accretionary wedge

The steeply-plunging geometry of the D_{3Gn} folds in the Bastar anatectic gneisses (Fig. 5b) are in sharp contrast (Fig. 5f) with the gently plunging D_{3SS} folds in the supracrustal belts (Fig. 5b). It follows that the D_{2Gn} fabric in the gneisses (steep-dipping; Fig. 5a) and the D_{2SS} fabric in the inter-layered micaceous quartzites and mica schists in the supracrustal unit (gently-dipping; Fig. 5b) prior to D_3 (D_{3Gn} is time equivalent to D_{3SS}) crustal shortening was oblique (Fig. 5f). This structural discordance in the pre-D_3 orientations in the two units is also evident in the dissimilar orientations of D_{2Gn} and D_{2SS} fold axis. The mineral paragenetic relations described earlier suggest that the sub-greenschist facies to amphibolite facies metamorphic conditions in schists prior to and during the formation of S_{2SS} in the supracrustal unit (Fig. 8) are in sharp contrast with the granulite facies conditions that prevailed in the Paleoproterozoic Bastar gneisses prior to and during S_{2Gn} (Fig. 6). Due to the pre-S_{2SS} structural-metamorphic discordance, we infer that the two lithodemic units involved in D_3 crustal shortening were tectonically accreted (Ghosh et al., 2016) post-D_2.

The ensemble of quartzite and mica schist, the intra-formational conglomerates and meta-ultramafic/mafic bands possibly constitute active margin setting fringing the Bastar/Singhbhum Cratons. The unsorted and the polymict nature of the clasts in the conglomerates, and the frequent occurrence of ultramafic schists at least in the northern schist belt suggest the supracrustal belt is likely to have been deposited in an accretionary wedge. The contrasting P–T paths retrieved for the schists culminating at varying peak P–T conditions in closely-spaced samples of varying bulk composition (Fig. 8d–e) are typical for exhumed

supracrustal units subducted to variable depths (Selverstone, 1985; Selverstone et al., 1984; Spear, 1989).

One of major problems in reconstructing the accretion age in the Rengali orogen is in interpreting the U–Pb and Pb–Pb ages obtained from zircon separates and in situ monazite age determinations in mica schists in the Rengali supracrustal belt. Resolving the significance of the multiple ages obtained in the supracrustal belt is not straightforward for two reasons. First, the zircon ages, or a majority of these, in the metasedimentary units in the supracrustal belt may correspond with those retrieved from detrital zircon grains; alternatively the supracrustal rocks may have experienced as many events, if the zircon grains are texturally identified to be non-detrital in origin (cf. Phillips et al., 2006). Second, experimental data on intra-crystalline diffusion in monazite suggests that solid state diffusion in monazite (as with zircon), is negligible at T < 750 °C (Cherniak et al., 2004; Gardès et al., 2006, 2007). Thus, monazites, as with zircon, once formed at T > 750 °C is minimally modified by intra-crystalline diffusion in response to lower-T deformation/metamorphic events (Gordon et al., 2009; Harlov et al., 2007; Rasmussen et al., 2005; Whitney et al., 2003). Unlike zircon, however, monazites readily grow during low-T metamorphism by fluid-aided dissolution and re-precipitation (Rasmussen and Muhling, 2007; Rasmussen et al., 2005; Rekha and Bhattacharya, 2013; Rekha et al., 2013a; Schärer et al., 1999), and therefore, in situ monazite age determinations is ideally suited for dating low-T metamorphic events (Janots et al., 2009; Rasmussen and Muhling, 2007; Rasmussen et al., 2001; Rekha et al., 2013b). Zircon, on the other hand, is likely to remain passive to these low-T metamorphic events (Gordon et al., 2009; Harlov et al., 2007; Kapp et al., 2005; Rasmussen et al., 2005; Whitney et al., 2003).

Chattopadhyay et al. (2015) report LA-ICPMS U–Pb and Pb–Pb zircon ages in two mica schists (S-26 and S-30) in the Rengali supracrustal belt. U–Pb and Pb–Pb zircon ages in the mica schist sample (S-26) are 2470 ± 23 Ma and 2471 ± 26 Ma respectively. The multiple populations of $^{207}Pb/^{206}Pb$ zircon ages are obtained in the mica schist sample S-30, e.g. 2867 ± 20 Ma, 2788 ± 25 Ma, 2423 ± 30 Ma and 937 ± 18 Ma. The zoning patterns in the zircon grains in the schists suggest the ages are likely to correspond with magmatic/metamorphic growth events, but the cathodoluminescence images (Fig. 9 of Chattopadhyay et al., 2015) show the zircon grains in the two samples to be anhedral with broken corners, and with margins typically angular, less commonly sub-rounded, and the grain interiors commonly pitted. These morphological features seem to suggest that the Early Neoarchean and older zircon grains in schists were detrital in nature. The U–Pb and Pb–Pb ages are therefore likely to correspond with inherited ages, and are unlikely to represent the metamorphic age of the supracrustal belt.

As in this study, monazite chemical ages in schists/quartzites in the supracrustal belt reported by Chattopadhyay et al. (2015) vary widely within a rock, and collectively in the supracrustal belt, e.g. 0.6–0.5 Ga, 0.85–0.80 Ga, 1.0–0.9 Ga, ca. 1.2 Ga, ~2.0 Ga and 2.5–2.4 Ga; the mean age of the most dominant populations occur at 0.55–0.50 Ga and 1.0–0.9 Ga, and a less prominent age population at 0.85–0.80 Ga. Based on the age data, Chattopadhyay et al. (2015) suggest the EGGB docked with the Singhbhum Craton during the Early Neoproterozoic, 1.0–0.9 Ga. The proposition appears untenable on several counts. First, the Early Neoproterozoic monazite ages in the Rengali supracrustal rocks coincides with the Grenvillian-age ultra high-T granulite facies metamorphism and contemporaneous emplacement of felsic intrusives in the EGGB (Aftallion et al., 1988; Biswal et al., 2007; Mezger and Cosca, 1999; this study). If so, one would expect the Rengali supracrustal rocks, at least those contiguous with the EGGB, to have experienced high-T metamorphism and anatexis, for which there is no evidence. If the eventual docking of the Rengali supracrustal rocks occurred in the wake of high-grade metamorphism-magmatism in the EGGB, one would still expect the supracrustal rocks to have experienced Grenvillian-age prograde heating synchronous with and post-dating the accretion fabric, and further, a progressive northward decrease in temperature is likely

to have been imposed within the Rengali supracrustal belt. No systematic N-S variation in metamorphic peak P–T condition has yet been established within the Rengali orogen. Instead deformation microtextures in sheared granitoids and mineral paragenetic relations in the Rengali supracrustal rocks suggest that the T_{max} values attained on accretion are unlikely to have exceeded 600 C. Second, available evidence from the Kantilo shear zone shows that the ca. 0.95 Ga high-grade metamorphism in the EGGB was overprinted by a Mid-Neoproterozoic (800–700 Ma) granulite facies event (cf. Dobmeier and Simmat, 2002; this study) marked by high-P, T conditions (850–900C and 8–10 Kbar). If the EGGB-SC accretion was indeed Grenvillian in age, it would be fortuitous for the Rengali supracrustal rocks to have escaped this high-T Mid-Neoproterozoic metamorphic event. Third, the re-orientation and transposition of N/NE-trending Grenvillian-aged tectonic fabric in the Gangpur schist belt at the contact with the WNW-trending Rengali orogen indicates that the Rengali orogen is younger. And, finally the lack of Grenvillian-age mantles around Paleoproterozoic and older cores in monazites (invariably rimmed by Pan African domains) in the Rengali schists suggests the supracrustal belt did not experience the Grenvillian-age accretion invoked by Chattopadhyay et al. (2015). One may argue that the Grenvillian-age mantles around the older cores were indeed present, but these mantles were subsequently obliterated by dissolution-precipitation processes linked to Pan African "reactivation". If so, one needs to explain as to why the Grenvillian-ages were selectively obliterated by the Pan African reactivation, while the older cores were preserved.

Summarizing, the assembly of the Neoproterozoic EGGB with the Bastar–Singhbhum Craton composite appears to have occurred during the Pan African. The older ages in the Rengali supracrustal belt, in all probability, correspond to detrital zircon and monazite grains derived from the neighboring Bastar (2.0–2.6 Ga; this study) and Singhbhum Cratons (dominantly 3.6–2.9 Ga, Prabhakar and Bhattacharya, 2013, and references there in), and the Grenvillian-age EGGB (Aftallion et al., 1988; Biswal et al., 2007; Mezger and Cosca, 1999; this study) and the GSB (1.0–0.9 Ga; this study) metamorphic belts.

9.4. The Antarctic connection

The Early Neoproterozoic (1.0–0.9 Ga) granulite facies metamorphism and juvenile crust formation ages in major parts of the EGGB are deemed to be similar to those in the Rayner Complex, Antarctica

(Black et al., 1987; Halpin et al., 2005; Kelly et al., 2002; Mezger and Cosca, 1999). Outcrops in the Prydz Bay region, Antarctica (Fig. 14) record Pan African high-grade metamorphism, magma emplacement and deformation (Carson et al., 1996; Fitzsimons et al., 1997; Hensen and Zhou, 1995, 1997; Kelsey et al., 2003, 2007; Kinny et al., 1997; Zhao et al., 1992, 2003). The Pan African tectonism demonstrably extends inland into the Grove Mountains (Liu et al., 2007; Mikhalsky et al., 2001) and westwards in the neighborhood of the Southern Prince Charles Mountains (Boger et al., 2000, 2001, 2008; Corvino et al., 2005, 2008). But barring the Paleoproterozoic gneisses in the Lambert graben, the rocks in these regions preserve an earlier ~1.0 Ga history that is correlated with events in the adjacent Rayner Complex (Grew et al., 2012; Wang et al., 2008). The peak P–T condition attained during the Pan African deformation in the Prydz Bay is in the range 6–8 kbar and 800–860 °C (Fitzsimons, 1996; Harley and Buick, 1992). The Pan African P–T conditions southwards in the Paleoproterozoic southern Lambert Complex are significantly lower at 5·8–6·1 kbar and 625–635 °C (Phillips et al., 2009). Eastwards across the Amery ice sheet, the effect of Pan African tectonism, albeit localized along strongly tectonized zones, extends till the ca. 1.0 Ga domains of the Rauer Group in the northern Prydz Bay, and in the Vestfold Hills Block that exhibits high-grade metamorphism and magmatism at ca. 2.5 Ga (Black et al., 1991; Liu et al., 2009, 2014, and references there in). The assembly of disparately evolved crustal domains in the northern Prydz Bay does not share a common history until 0.5 Ga (Harley et al., 1998; Kinny et al., 1993). East of the Vestfold Block, 1.0 Ga tectonism is lacking, but Pan Africa tectonism is manifested by ca. 0.5 Ga charnockites in the Mirny Station (McQueen et al., 1972), 0.5 Ga charnockite and syenite intrusion within Archean orthogneisses west of the Denman Glacier (Harley et al., 2013), and weak 0.5 Ga overprinting of Mesoproterozoic high-grade gneisses in the east of Denman Glacier (Post et al., 1997) proximally located to the Darling Fault in western Australia.

The Archean-Early Paleoproterozoic events are also evident in the neighborhood of the Southern Prince Charles Mountains, e.g. in the Archean Ruker Complex records igneous events at ca. 3.2 and ca. 2.8 Ga, whereas magmatic and high-grade metamorphic events of the Lambert Complex occurred at 2.4 Ga and 2.1 Ga. The Lambert complex records a 1.0 Ga metamorphic overprint (Corvino et al., 2008) suggesting its Early Neoproterozoic accretion with the adjacent Rayner Complex (Harley et al., 2013); but both the Lambert and the Rucker complexes exhibit strong amphibolite facies overprinting at ~0.5 Ga (Corvino et al.,
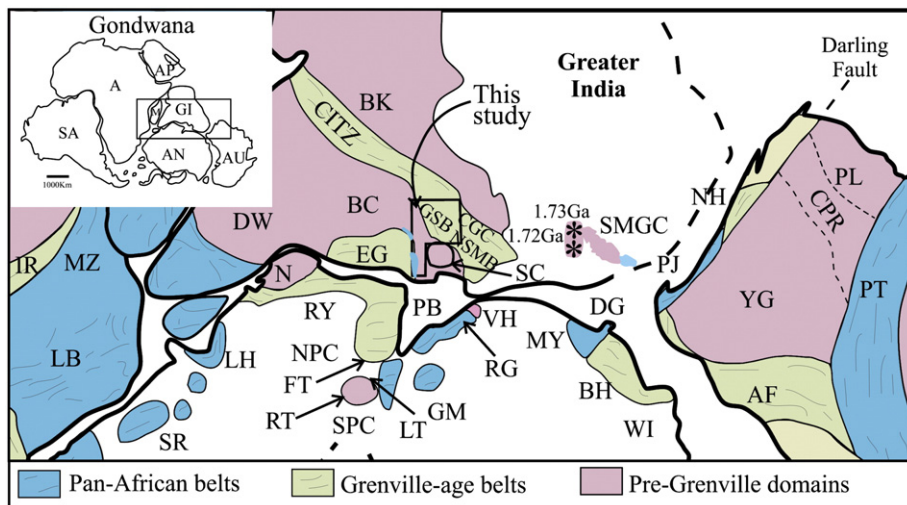
Fig. 14. Pan African (~0.5 Ga) and Grenvillian-age (0.9–1.0 Ga) belts in Greater India and parts of the Australo–Antarctic Block (modified after Harley et al., 2013). The study area, encompassing parts of the Rengali orogen, is shown in box. Acronyms (India): CGC—Chottanagpur Gneiss Complex, CITZ—Central India Tectonic Zone, EG—Eastern Ghats Granulite Belt, GSB—Gangpur Schist Belt, NSMB—North Singhbhum Mobile Belt, SC—Singhbhum Craton, SMGC—Shillong Meghalaya Gneiss Complex. Acronyms (Antarctica): LT—Lambert terrane, RT—Rucker terrane, FT—Fisher terrane. The remaining abbreviations are the same as in Harley et al. (2013). Stars with numbers indicate the locations and SHRIMP ages (in Ga) in Paleoproterozoic granitoids obtained in drill cores in NW Bangladesh (Ameen et al., 2007; Hossain et al., 2007).

2008; Phillips et al., 2009). Low-grade metasedimentary rocks comprising quartzites, phyllites, micaceous quartzites and intra-formational conglomerates, are reported from several localities (Mt. Rubin, Mt. Maguair and the Compston massif) in the Ruker Complex. These metasedimentary units share tectonized contact with the metamorphosed older gneisses (Mikhalsky, 2007; Phillips et al., 2006), and contains multiple age populations of detrital zircon, e.g. 2.6 Ga, 2.2 Ga and 1.1–1.0 Ga (Phillips et al., 2006), thereby suggesting a Neoproterozoic depositional age for the sediments (Mikhalsky, 2007). The two granite-gneiss and three phyllite samples from Mt. Rubin yield a Rb–Sr whole isochron age of 505 ± 40 Ma, inferred to be the age of metamorphic reorganization of the sediments (Mikhalsky, 2007; Phillips et al., 2006).

In the eastern India Precambrian complexes, Pan African U–Pb zircon and monazite chemical ages are reported within the Grenvillian-age domain in the EGGB (Krause et al., 2001; Mezger and Cosca, 1999) and prominently along the cratonic interface with EGGB (Aftalion et al., 2000; Biswal et al., 2007; Upadhyay, 2008, and references therein; this study). Several lines of evidence suggest that Pan African tectonism at the EGGB-craton interface occurred at upper amphibolite facies conditions. Bhadra et al. (2007) demonstrated westward thrusting of EGGB over the cratonic hinterland induced polyphase dynamic melting in cratonic granites in and around Ranmal (Fig. 1) along the NW margin of the EGGB; in the area, a correlated decrease in strain and temperature distal from the EGGB-craton accretion zone was documented by Bhadra et al. (2003). Biswal et al. (2007) retrieved Pan African U–Pb ages in the Khariar meta-syenite (Fig. 1) emplaced synchronous with the EGGB-Bastar Craton accretion. The P–T conditions of syn-thrusting felsic melt generation at the EGGB-craton interface is corroborated by Pan African high-T metamorphism (5.5–7.0 kbar and 600–700 °C) retrieved by Upadhyay and Raith (2006) from coronal garnet mantling orthopyroxene–clinopyroxene–ilmenite aggregates in metasyenite near Kondapalle. These evidences, and the absence of Grenvillian-age metamorphic and magmatic episodes in the Archean/Paleoproterozoic Bastar Craton fringing the EGGB, indicate that the EGGB and the craton did not share a common history until the two crustal domains were juxtaposed during the Pan African.

It appears that a Pan African tectonic front along the northern marhin of the EGGB (Rengali orogen) and the western margin of the EGGB in eastern India extends eastwards towards the Prydz Bay region in Antarctica (Fig. 14). In the Shillong-Meghalaya Gneiss Complex, NE India (Fig. 14), another Pan African tectonic front in the Sonapahar region is manifested by 0.5 Ga granulite facies metamorphism and felsic magmatism that overprint the Mesoproterozoic (1.7–16 Ga) gneisses (Chatterjee et al., 2008, 2011). This domain possibly demarcates the western margin of the Pan African tectonic front to the west of Mirny Station, Denman Glacier and the Darling Fault (Fig. 14). The SSW structural trend of the Pan African tectonic front sub-parallel to the Darling Fault possibly extended towards the Prydz Bay region, but the southward extension of the front is possibly obscured by the expansive Gangetic alluvial deposits overlying the crystalline basement in the southern part of Bangladesh.

In crustal domains within eastern India straddled by the two Pan African tectonic fronts, there is no evidence of Pan African tectonism, e.g. in the Singhbhum Craton (Basu et al., 1996; Mishra et al., 1999; Prabhakar, 2013; Prabhakar and Bhattacharya, 2013; Sharma et al., 1994), and in the Meso/Early Neoproterozoic crustal domains of NSMB and CGC (Fig. 14). In NW Bangladesh, SHRIMP U–Pb zircon age determinations in drill core samples indicate the occurrence of 1.72–1.73 Ga granitoids (Ameen et al., 2007; Hossain et al., 2007), but again, Pan African ages are lacking in the drill core samples in NW Bangladesh. Overall, it appears that Pan African tectonic front in eastern India and Bangladesh straddle the facing coast lines of the Australo-Antarctic Block and the Greater India Block (Fig. 14) in a Pan Gondwana set-up (Collins and Pisarevsky, 2005; Li et al., 2008). We suggest that the Pan African accretion front located along the northern margin (Rengali orogen) and continuing along the western margin of the Grenvillian-age domain in EGGB (a dismembered part of the Rayner Complex) is

the locus along which the EGGB integrated with the Greater India land-mass as late as the Pan African, coinciding with the final assembly of the Gondwanaland.

Supplementary data to this article can be found online at http://dx.doi.org/10.1016/j.lithos.2016.06.006.

Appendix A. Locations (latitude, longitude) of samples used for estimating metamorphic conditions (locations of monazite/zircon-dated samples in Fig. 13)

J-54	(22°10.87′N, 84°11.88′E)
J-416B	(21°27.55′N, 84°29.53′E)
J-469	(21°23.03′N, 84°10.10′E)
TC-99B	(21°07.02′N, 85°27.42′E)
TC-08	(21°05.83′N, 85°28.23′E)
TC-67	(21°08.79′N, 85°03.79′E)
PH-9B	(21°06.04′N, 85°07.30′E)
PH-10	(21°06.22′N, 84°11.48′E)
NY9A, B	(20°22.36′N, 85°07.41′E)

Appendix B. P–T pseudosection reconstruction

P–T pseudosections were constructed using the Perple_X (version 6.6) after Connolly (2009). The following solution models (in parenthesis) listed in the data base of the program for constructing the P–T pseudosections, e.g. chloritoid [ctd(HP)], chlorite [chl(HP)], staurolite [St(HP)], garnet [Gt(HP)], muscovite [Pheng(HP)], biotite [Bio(TCC)], orthopyroxene [opx(HP)], clinopyroxene [cpx(HP)], plagioclase [Fsp(C1)], melt [melt(HP)] and cordierite [Crd(HP)]. Aluminosilicate polymorphs, quartz and K-feldspar were taken to be condensed phases. In the computations, H_2O was taken to be a pure phase; the Compensated–Redlich–Kwong equation for H_2O after Holland and Powell (1991) was adopted in the computations.

Appendix C. Analytical conditions and data processing for monazite age determinations

Monazite age determinations following Montel et al. (1996) were performed using a CAMECA SX-100 electron probe microanalyzer unit in the Department of Geology and Geophysics, Indian Institute of

Technology, Kharagpur. Four samples from the Kantillo shear zone was analyzed by JEOL-JXA-8200 Superprobe at Department of Earth and Planetary Sciences, Massachusetts Institute of Technology. The operating conditions using SX-100, the analytical protocol, and the data reduction methodology are adopted from Prabhakar (2013). For spot age determination, monazite grains larger than 5 μm diameter were chosen to eliminate effects induced by grain boundary defects in smaller grains; also, monazite grains with at least 3.5 wt.% ThO_2 were analyzed because at lower ThO_2 abundances the 2σ error on spot age increases dramatically (Prabhakar, 2013). The 2σ error of spot ages in the analyzed monazites varies between 2 and 10% of the absolute age (cf. Prabhakar, 2013); error % of the overwhelming majority (>80%) of spot ages is <7% (Supplementary Material 7). Isoplot 3.75 (Ludwig, 2012) was used for estimating population ages in chemically distinct domains in monazites. The analytical conditions and data reduction procedures for the JEOL-JXA superprobe are outlined in Chatterjee et al. (2010, 2011).

Appendix D. SIMS U–Pb and Pb–Pb (zircon) age determination

U–Pb zircon age determinations were performed with a CAMECA ims1270 ion microprobe at University of California, Los Angeles using a ca. 15 nA O-primary beam focused to a ~30 μm spot. Analyses were done on araldite-mounted zircon grain separates in four samples, J-180A, 240, 307, 309. The details of analytical conditions are provided in Mojzsis et al. (2003). The zircon age standard AS3 (1099 ± 1 Ma, Paces and Miller, 1993) was used for age calibrations (Supplementary Material 8). The concentrations of Th and U were determined by comparison with the zircon trace element standard 91,500 (Wiedenbeck et al., 2004). Quoted external errors include both the internal error for individual data points and the uncertainty of the calibration curve. The 1σ error of spot $^{206}Pb/^{238}U$ ages in the analyzed zircons varies between 2 and 6% of the absolute age (two measurements, one each in J-240 and J-180A, show higher error at 7%; Table 1). The dominant majority (25 out 26) of $^{207}Pb/^{235}U$ age errors in the analyzed zircons varies between 1 and 4% of the absolute age (Table 1); one measurement in J-240 has 5% 1σ-error (Table 1). The 1σ-error of $^{207}Pb/^{206}U$ (zircon) ages is ≤1% (Table 1).

References

Aftalion, M., Bowes, D.R., Dash, B., Fallick, A.E., 2000. Late Pan-African thermal history in the Eastern Ghats terrane India from U–Pb and K-Ar isotopic study of the Mid-Proterozoic Khariar alkali syenite Orissa. Proceedings of Precambrian Crust in Eastern and Central India IGCP-368. (Geological Survey of India, Calcutta), Bhubaneswar, pp. 26–33.

Aftallion, M., Bowes, D.R., Dash, B., Dempster, T.J., 1988. Late Proterozoic charnockites in Orissa, India: a U–Pb and Rb-Sr isotopic study. Journal of Geology 96, 663–676.

Ahmad, T., Kaulina, T.V., Wanjari, N., Mishra, M.K., Nitkina, E.A., 2009. U–Pb zircon chronology and Sm–Nd isotopic characteristics of the Amgaon and Tirodi Gneissic Complex, Central Indian Shield: constraints on Precambrian crustal evolution. In: Singh, V.K., Chandra, R. (Eds.), Precambrian Continental Growth and Tectonism. Excel India Publishers, New Delhi, pp. 137–138.

Altenberger, U., Wilhelm, S., 2000. Ductile deformation of K-feldspar in dry eclogite facies shear zones in the Bergen arcs, Norway. Tectonophysics 320, 107–121.

Ameen, S.M.M., Wilde, S.A., Kabir, M.Z., Akon, E., Chowdhury, K.R., Khan, M.S.H., 2007. Paleoproterozoic granitoids in the basement of Bangladesh: a piece of the Indian shield or an exotic fragment of the Gondwana jigsaw? Gondwana Research 12, 380–387.

Aranovich, L.Y.A., Berman, R.G.B., 1997. A new garnet-orthopyroxene thermometer based on reversed Al_2O_3 solubility in $FeO–Al_2O_3–SiO_2$ orthopyroxene. American Mineralogist 82, 345–353.

Bandyopadhyay, B.K., Bhoskar, Ramachandra, H.M., Roy, A., Khadse, V.K., Mohan, M., Barman, T., Bishui, P.K., Gupta, S.N., 1990. Recent geochronological studies in parts of the Precambrian of Central India. Geological Survey of India Special Publication 28, 199–210.

Banerjee, P.K., 1967. Revision of stratigraphy, structure and metamorphic history of the Gangpur series, Sundergarh District, Orissa. Records of the Geological Survey of India 95, 327–346.

Basu, A.R., Sharma, M., Premo, W.R., 1996. U–Pb age of an Older Metamorphic Group Mica Schist: earliest terrain of the eastern Indian Craton. In: Saha, A.K. (Ed.), Recent Researches in Geology and Geophysics of the Precambrians. Hindustan Publication Corporation, New Delhi, India, pp. 93–102.

Bhadra, S., Banerjee, M., Bhattacharya, A., 2003. Tectonic restoration of a polychronous mobile belt-craton assembly: constraints from corridor study across the western margin of the eastern Ghats Belt, India. Memoirs Geological Society of India 109–130.

Bhadra, S., Das, S., Bhattacharya, A., 2007. Shear zone-hosted migmatites (eastern India): the role of dynamic melting in the generation of REE-depleted felsic melts, and implications for disequilibrium melting. Journal of Petrology 48, 435–457.

Bhattacharya, S., 1997. Evolution of eastern Ghats granulite belt of India in a compressional tectonic regime and juxtaposition against iron ore craton of Singhbhum by oblique collision-transpression. Proceedings of the Indian Academy of Sciences (Earth and Planetary Sciences) 106, 65–75.

Bhattacharya, S., 2002. Nature of crustal tri-junction between the eastern Ghats mobile belt, Singhbhum craton and Bastar craton around Paikmal, western Orissa: structural evidence of oblique collision. Gondwana Research 5, 53–62.

Bhattacharya, A., Krishnakumar, K.R., Raith, M., Sen, S.K., 1991. An improved set of a- X parameters for Fe-Mg-Ca garnets and refinement of the orthopyroxene–garnet–plagioclase–quartz barometer. Journal of Petrology 32, 629–656.

Bhattacharya, A., Mohanty, L., Maji, A., Sen, S.K., Raith, M., 1992. Non-ideal mixing in the phlogopite-annite boundary: constraints from experimental data on Mg-Fe partitioning and reformulation of the biotite-garnet geothermometer. Contributions to Mineralogy and Petrology 111, 87–93.

Biswal, T.K., 2000. Fold-thrust belt geometry of eastern Ghats Mobile Belt — a structural study from its western margin Orissa India. Journal of African Earth Sciences Special 31, 25–33.

Biswal, T.K., De Waele, B., Ahuja, H., 2007. Timing and dynamics of the juxtaposition of the eastern Ghats Mobile Belt against the Bhandara craton, India: a structural and zircon U–Pb SHRIMP study of the fold-thrust belt and associated nepheline syenite plutons. Tectonics 26, TC4006. http://dx.doi.org/10.1029/2006TC002005.

Black, L.P., Harley, S.L., Sun, S.S., McCulloch, M.T., 1987. The Rayner complex of East Antarctica: complex isotopic systematics within a Proterozoic mobile belt. Journal of Metamorphic Geology 5, 1–26.

Black, L.P., Kinny, P.D., Sheraton, J.W., Delor, C.P., 1991. Rapid production and evolution of late Archaean felsic crust in the Vestfold block of East Antarctica. Precambrian Research 50, 283–310.

Boger, S.D., Carson, C.J., Wilson, C.J.L., Fanning, C.M., 2000. Neoproterozoic deformation in the Radok Lake region of the northern Prince Charles mountains, East Antarctica: evidence for a single protracted orogenic event. Precambrian Research 104, 1–24.

Boger, S.D., Wilson, C.J.L., Fanning, C.M., 2001. Early Palaeozoic tectonism within the East Antarctic craton: the final suture between east and west Gondwana? Geology 29, 463–466.

Boger, S.D., Maas, R., Fanning, C.M., 2008. Isotopic and geochemical constraints on the age and origin of granitoids from the central Mawson escarpment, southern Prince Charles mountains, East Antarctica. Contributions to Mineralogy and Petrology 155, 379–400.

Bose, S., Das, K., Kimura, K., Hayasaka, Y., Hidaka, H., Dasgupta, A., Ghosh, G., Mukhopadhyay, J., 2013. Zircon and monazite geochronology of the granulites and associated gneisses from the Rengali Province, India: Growth of the Southern margin of the Singhbhum Craton. Abs. American Geophysical Union, Fall Meeting 2013, Abstract #V33D–2793.

Bose, S., Guha, V., Ghosh, G., Das, K., Mukhopadhyay, J., 2014. Tectonic juxtaposition of crust and continental growth during orogenesis: example from the Rengali Province, eastern India. Geoscience Frontiers http://dx.doi.org/10.1016/j.gsf.2014.09.002.

Cannat, M., Casey, J.F., 1995. An ultramafic lift at the Mid-Atlantic Ridge: successive stages of magmatism in serpentinized peridotites from the 15°N region. In: Nicholas, A. (Ed.), Vissers, R.L.M.Kluwer Academic Publications, Mantle and lower crust exposed in oceanic ridges and ophiolites, pp. 5–34

Cao, S.Y., Liu, J.L., Ling, H.U., 2007. Micro- and submicrostructural evidence for high-temperature brittle-ductile transition deformation of hornblende: case study of high-grade mylonites from Diancangshan, western Yunnan. Science in China, Series D (Earth Sciences) 50, 1459–1470.

Carson, C.J., Fanning, C.M., Wilson, C.J.L., 1996. Timing of the progress granite, Larsemann Hills: additional evidence for early Palaeozoic orogenesis within the East Antarctic shield and implications for Gondwana assembly. Australian Journal of Earth Sciences 43, 539–553.

Chatterjee, N., Mazumdar, A.C., Bhattacharya, A., Saikia, R.R., 2008. Mesoproterozoic granulites of the Shillong–Meghalaya plateau: evidence of westward continuation of the Prydz Bay pan-African suture into northeastern India. Precambrian Research 152, 1–26.

Chatterjee, N., Banerjee, M., Bhattacharya, A., Maji, A.K., 2010. Monazite chronology, metamorphism-anatexis and tectonic relevance of the mid-Neoproterozoic eastern Indian tectonic zone. Precambrian Research 179, 99–120.

Chatterjee, N., Bhattacharya, A., Duarah, B.P., Mazumdar, A.C., 2011. Late Cambrian reworking of paleo-Mesoproterozoic granulites in Shillong-Meghalaya gneissic complex (Northeast India): evidence from PT pseudosection analysis and monazite chronology and implications for east Gondwana assembly. Journal of Geology 119, 311–330.

Chattopadhyay, S., Upadhyay, D., Nanda, J.K., Mezger, K., Pruseth, K.L., Berndt, J., 2015. Proto-India was a part of Rodinia: evidence from Grenville-age suturing of the eastern Ghats Province with the Paleoarchean Singhbhum craton. Precambrian Research http://dx.doi.org/10.1016/j.precamres.2015.05.030.

Chaudhuri, A.K., Pal, A.B., 1977. Superposed folding in the northern part of the Gangpur series, Orissa. Journal of the Geological Society of India 18, 233–239.

Chaudhuri, A.K., Pal, A.B., 1982. Three phases of folding with macroscopic axial plane folding in the Gangpur Group in Eastern India. Recent Researches in Geology: Structure and Tectonics of the Precambrian Rocks. Hindustan Publishing Corporation, New Delhi, India.

Chaudhuri, A.K., Pal, A.B., Roy, A., 1980. Evidences of multiple deformations near Amaidegri in the western part of the Gangpur group. Journal of the Geological Society of India 21, 617–622.

Cherniak, D.J., Watson, E.B., Grove, M., Harrison, T.M., 2004. Pb diffusion in monazite: a combined RBS/SIMS study. Geochimica et Cosmochimica Acta 68, 829–840.

Chetty, T.R.K., 2014. Deep crustal shear zones in the eastern Ghats Mobile Belt, India: Gondwana correlations. Journal of the Indian Geophysical Union 18, 19–56.

Chowdhury, S., Lentz, D.R., 2011. Mineralogical and geochemical characteristics of scheelite-bearing skarns, and genetic relations between skarn mineralization and petrogenesis of the associated granitoid pluton at Sargipali, Sundergarh District, eastern India. Journal of Geochemical Exploration 108, 39–61.

Collins, A.S., Pisarevsky, S.A., 2005. Amalgamating eastern Gondwana: the evolution of the Circum-Indian orogens. Earth Science Reviews 71, 229–270.

Connolly, J.A.D., 2009. The geodynamic equation of state: what and how? Geochemistry, Geophysics, Geosystems 10, Q10014. http://dx.doi.org/10.1029/2009GC002540.

Cook, K.L., Royden, L.H., 2008. The role of crustal strength variations in shaping orogenic plateaus, with application to Tibet. Journal of Geophysical Research 13, 1–18.

Corvino, A.F., Boger, S.D., Wilson, C.J.L., Fitzsimons, I.C.W., 2005. Geology and SHRIMP U–Pb zircon chronology of the Clemence massif, central Prince Charles mountains, East Antarctica. Terra Antarctica 12, 55–68.

Corvino, A.F., Boger, S.D., Henjes-Kunst, F., Wilson, C.J.L., Fitzsimons, I.C.W., 2008. Superimposed tectonic events at 2450 Ma, 2100 Ma, 900 Ma and 500 Ma in the north Mawson escarpment, Antarctic Prince Charles mountains. Precambrian Research 167, 281–302.

Crowe, W.A., Cosca, M.A., Harris, L.B., 2001. $^{40}Ar/^{39}Ar$ geochronology and Neoproterozoic tectonics along the northern margin of the eastern Ghats belt in North Orissa, India. Precambrian Research 108, 237–266.

Crowe, W.A., Nash, C.R., Harris, L.B., Leeming, P.M., Rankin, L.R., 2003. The geology of the Rengali Province: implications for the tectonic development of northern Orissa, India. Journal of Asian Earth Sciences 21, 697–710.

Das, S., Nasipuri, P., Bhattacharya, A., Swaminathan, S., 2008. The thrust-contact between the eastern Ghats Belt and the adjoining Bastar craton (eastern India): evidence from mafic granulites and tectonic implications. Precambrian Research 162, 70–85.

Deogarh Quadrangle Map, 2003. Published by the Geological Survey of India.

Dobmeier, C.J., Simmat, R., 2002. Post-Grenvillean transpression in the Chilka Lake area, eastern Ghats Belt - implications for the geological evolution of peninsular India. Precambrian Research 113, 243–268.

Dobmeier, C., Lutke, S., Hammerschmidt, K., Mezger, K., 2006. Emplacement and deformation of the Vinukonda metagranite (eastern Ghats India): implications for the geological evolution of peninsular India and for Rodinia reconstructions. Precambrian Research 146, 165–178.

Ferry, J.M., Spear, F.S., 1978. Experimental calibration of the partitioning of Fe and Mg between biotite and garnet. Contributions to Mineralogy and Petrology 66, 113–117.

Fitzsimons, I.C.W., 1996. Metapelitic migmatites from Brattstrand bluffs, East Antarctica -metamorphism, melting and exhumation of the mid crust. Journal of Petrology 37, 395–414.

Fitzsimons, I.C.W., Kinny, P.D., Harley, S.L., 1997. Two stages of zircon and monazite growth in anatectic leucogneiss: SHRIMP constraints on the duration and intensity of pan-African metamorphism in Prydz Bay, East Antarctica. Terra Nova 9, 47–51.

Ganguly, J., Saxena, S.K., 1984. Mixing properties of aluminosilicate garnets; constraints from natural and experimental data, and applications to geothermo-barometry. American Mineralogist 69, 88–97.

Gapais, D., 1989. Shear structures within deformed granites: mechanical and thermal indications. Geology 17, 1144–1147.

Gardès, E., Jaoul, O., Montel, J.M., Seydoux-Guillaume, A.M., Wirth, R., 2006. Pb diffusion in monazite: an experimental study of Pb + Th = 2Nd interdiffusion. Geochimica et Cosmochimica Acta 70, 2325–2336.

Gardès, E., Montel, J.M., Seydoux-Guillaume, A.M., Wirth, R., 2007. Pb diffusion in monazite: new constraints from the experimental study of Pb2 + Ca2 + interdiffusion. Geochimica et Cosmochimica Acta 71, 4036–4043.

Ghosh, S.K., Sen, G., Sengupta, S., 2003. Rotation of long tectonic clasts in transpressional shear zones. Journal of Structural Geology 25, 1083–1096.

Ghosh, G., Bose, S., Das, K., Dasgupta, A., Takafumi, Y., Hayasaka, Y., Chakrabarti, K., Mukhopadhyay, J., 2016. Transpression and juxtaposition of middle crust over upper crust forming a crustal scale flower structure: insight from structural, fabric, and kinematic studies from the Rengali Province, eastern India. Journal of Structural Geology. http://dx.doi.org/10.1016/j.jsg.2015.12.006.

Gordon, S.M., Grove, M., Whitney, D.L., Schmitt, A.K., Teyssier, C., 2009. Time–temperature-fluid evolution of migmatite dome crystallization: coupled U–Pb age, Ti thermometry, and O isotopic ion microprobe depth profiling of zircon and monazite. Chemical Geology 262, 186–201.

Grew, E.S., Carson, C.J., Christy, A.G., Maas, R., Yaxley, G.M., Boger, S.D., Fanning, C.M., 2012. New constraints from U–Pb, Lu–Hf and Sm–Nd isotopic data on the timing of sedimentation and felsic magmatism in the Larsemann Hills, Prydz Bay, East Antarctica. Precambrian Research 206–207, 87–108.

Halpin, J.A., Gerakiteys, C.L., Clarke, G.L., Belousova, E.A., Griffin, W.L., 2005. In-situ U–Pb geochronology and Hf isotope analyses of the Rayner complex, East Antarctica. Contributions to Mineralogy and Petrology 148, 689–706.

Harley, S.L., 1984. An experimental study of the partitioning of Fe and Mg between garnet and orthopyroxene. Contributions to Mineralogy and Petrology 86, 359–373.

Harley, S.L., Buick, I.S., 1992. Wollastonite-scapolite assemblages as indicators of granulite pressure–temperature-fluid histories: the Rauer group, East Antarctica. Journal of Petrology 33, 693–728.

Harley, S.L., Snape, I., Black, L.P., 1998. The evolution of a layered metaigneous complex in the Rauer group, East Antarctica: evidence for a distinct Archaean terrane. Precambrian Research 89, 175–205.

Harley, S.L., Fitzsimons, I.C.W., Zhao, Y., 2013. Antarctica and supercontinent evolution: historical perspectives, recent advances and unresolved issues. Geological Society of London, Special Publication 383, 1–34.

Harlov, D.E., Wirth, R., Hetherington, C.J., 2007. The relative stability of monazite and huttonite at 300–900 °C and 200–1000 MPa: metasomatism and the propagation of metastable mineral phases. American Mineralogist 92, 1652–1664.

Hensen, B.J., Zhou, B., 1995. A pan-African granulite facies metamorphic episode in Prydz Bay, Antarctica: evidence from Sm–Nd garnet dating. Australian Journal of Earth Sciences 42, 249–258.

Hensen, B.J., Zhou, B., 1997. East Gondwana Amalgamation by Pan-African Collision? Evidence from Prydz Bay, East Antarctica. In: Ricci, C.A. (Ed.), The Antarctic Region: Geological Evolution and Processes. Terra Antarctica Publications, Siena, pp. 115–119.

Hippe, K., Möller, A., von Quadt, A., Peytcheva, I., Hammerschmidt, K., 2015. Zircon geochronology of the Koraput alkaline complex: insights from combined geochemical and U–Pb–Hf isotope analyses, and implications for the timing of alkaline magmatism in the eastern Ghats Belt, India. Gondwana Research. http://dx.doi.org/10.1016/j.gr.2015.02.021.

Hodges, K.V., Spear, F.S., 1982. Geothermometry, geobarometry and the Al_2SiO_5 triple point at Mt. Moosilauke, New Hampshire. American Mineralogist 67, 1118–1134.

Hodges, K.V., Crowley, P.D., 1985. Error estimation empirical geothermobarometry for pelitic systems. American Mineralogist 70, 702–709.

Holland, T.J.B., Powell, R., 1991. A compensated-Redlich-Kwong (CORK) equation for volumes and fugacities of CO2 and H20 in the range 1 bar to 50 kbar and 100–1600 °C. Contributions to Mineralogy and Petrology 109, 265–273.

Hoskin, P.W., Schaltegger, U., 2003. The composition of zircon and igneous and metamorphic petrogenesis. Reviews in Mineralogy and Geochemistry 53, 27–62.

Hossain, I., Tsunogae, T., Rajesh, H.M., Chen, B., Arakawa, Y., 2007. Palaeoproterozoic U–Pb SHRIMP zircon age from basement rocks in Bangladesh: a possible remnant of the Columbia supercontinent. Comptes Rendus Geoscience. http://dx.doi.org/10.1016/j.crte.2007.09.014.

Indares, A., Martignole, J., 1985. Biotite-garnet geothermometry in the granulite facies: the influence of Ti and Al in biotite. American Mineralogist 70, 272–278.

Jamieson, R.A., Beaumont, C., Nguyen, M.H., Culshaw, N.G., 2007. Synconvergent ductile flow in variable-strength continental crust: numerical models with application to the western Grenville orogen. Tectonics 22. http://dx.doi.org/10.1029/2006TC002036.

Janots, E., Engi, M., Rubatto, D., Berger, A., Gregory, C., Rahn, M., 2009. Metamorphic rates in collisional orogeny from in situ allanite and monazite dating. Geology 37, 11–14.

Kanungo, D.N., Mahalik, N.K., 1975. A revision of the stratigraphy and structure of Gangpur series in Sundergard District. Orissa and their tectonic history. Misccellaneous Publications of the Geological Survey of India 23, 130–137.

Kapp, J.L.D., Harrison, T.M., Kapp, P.A., Grove, M., Lovera, O.M., Lin, D., 2005. The Nyaingentanglha Shan: a window into the tectonic, thermal, and geochemical evolution of the Lhasa block, southern Tibet. Journal of Geophysical Research 110, B08413.

Kelly, N.M., Clarke, G.L., Fanning, C.A.M., 2002. A two-stage evolution of the Neoproterozoic Rayner structural episode: new U–Pb sensitive high resolution ion microprobe constraints from the Oygarden group, Kemp land, East Antarctica. Precambrian Research 116, 307–330.

Kelsey, D.E., Powell, R., Wilson, C.J.L., Steele, D.A., 2003. (Th + U)–Pb monazite ages from Mg– Al-rich metapelites, Rauer group, East Antarctica. Contributions to Mineralogy and Petrology 146, 326–340.

Kelsey, D.E., Hand, M., Clark, C., Wilson, C.J.L., 2007. On the application of in situ monazite chemical geochronology to constraining P–T–t histories in high-temperature (.850 8C) polymetamorphic granulites from Prydz Bay, East Antarctica. Journal of the Geological Society of London 164, 667–683.

Kinny, P.D., Black, L.P., Sheraton, J.W., 1993. Zircon ages and the distribution of Archaean and Proterozoic rocks in the Rauer Islands. Antarctic Science 5, 193–206.

Kinny, P.D., Black, L.P., Sheraton, J.W., 1997. Zircon U–Pb ages and geochemistry of igneous and metamorphic rocks in northern Prince Charles mountains, Antarctica. Journal of Australian Geology and Geophysics 16, 637–654.

Klemperer, S.L., 2006. Crustal flow in Tibet: Geophysical evidence for the physical state of Tibetan lithosphere, and inferred patterns of active flow. In: Law, R.D., Searle, M.P., Godin, L. (Eds.), Channel Flow. Ductile Extrusion and Exhumation in Continental Collision Zones. Geological Society of London Special Publications Vol. 268, pp. 39–70.

Koons, P.O., Crawl, D., Cox, S.C., Upton, P., Templeton, A.S., Chamberlain, C.P., 1998. Fluid flow during active oblique convergence: a southern alps model from mechanical and geochemical observations. Geology 26, 159–162.

Krause, O., Dobmeier, C., Raith, M.M., Mezger, K., 2001. Age of emplacement of massif-type anorthosites in the eastern Ghats Belt, India: constraints from U–Pb zircon dating and structural studies. Precambrian Research 109, 25–38.

Krishnamurthy, P., Chaki, A., Pandey, B.K., Chimote, J.S., 1988. Geochronology of the granite-rhyolite suites of the Dongargarh Supergroup, Central India. Proceedings of the 4th National Symposium on mass spectrometry, Bangalore. Earth and Planetary Science 2, 1–5.

Kruhl, J.H., 1996. Prism- and basal-plane parallel subgrain boundaries in quartz: a microstructural geothermobarometer. Journal of Metamorphic Geology 14, 581–589.

Lee, S.M., Ganguly, J., 1988. Equilibrium compositions of coexisting garnet and orthopyroxene: experimental determination in the system $FeO–MgO–Al_2O_3–SiO_2$, and applications. Journal of Petrology 29, 93–113.

Lee, P.E., Jessup, M.J., Shawb, C.A., Hicks, G.L., Allen, G.L., 2012a. Strain partitioning in the mid-crust of a transpressional shear zone system: insights from the Homestake and slide Lake shear zones, Central Colorado. Journal of Structural Geology. http://dx.doi.org/10.1016/j.jsg.2012.02.006.

Lee, S.Y., Min, K., Ree, J.-H., Jan, R., Jung, H., 2012b. The Geounri shear zone in the Paleozoic Taebaeksan Basin of Korea: tectonic implications. Journal of Structural Geology 42, 91–103.

Li, Z.X., Bogdanova, S.V., Collins, A.S., Davidson, A., De Waele, B., Ernst, R., Evans, D., Fitzsimons, I.C.W., Fuck, R.A., Gladkochub, D.P., Jacobs, J., Karlstrom, K.E., Lu, S., Natapov, L., Pease, V., Pisarevsky, S.A., Thrane, K., Vernikovsky, V., 2008. Assembly, configuration, and break-up history of Rodinia: a synthesis. Precambrian Research 160, 179–210.

Lisker, F., Fachmann, S., 2001. Phanerozoic history of the Mahanadi region, India. Journal of Geophysical Research 106. http://dx.doi.org/10.1029/2001JB000295.

Liu, X.C., Jahn, B.-M., Zhao, Y., Zhao, G.C., Lui, X.H., 2007. Geochemistry and geochronology of highgrade rocks from the Grove Mountains, East Antarctica: evidence for an early Neoproterozoic basement metamorphosed during a single late Neoproterozoic/Cambrian tectonic cycle. Precambrian Research 158, 93–118.

Liu, X.C., Zhao, Y., Song, B., Liu, J., Cui, J., 2009. SHRIMP U–Pb zircon geochronology of high-grade rocks and charnockites from the eastern Amery ice shelf and southwestern Prydz Bay, East Antarctica: constraints on late Mesoproterozoic to Cambrian tectonothermal events related to supercontinent assembly. Gondwana Research 16, 342–361.

Liu, X., Jahn, C., B-M., Zhao, Y., Liu, J., Ren, L., 2014. Geochemistry and geochronology of Mesoproterozoic basement rocks from the eastern Amery ice shelf and southwestern Prydz Bay, east Antractica: implications for a long-lived magmatic accretion in a continental arc. American Journal of Science 314, 508–547.

Ludwig, K.R., 2012. Isoplot 3.75: a Geochronological Toolkit for Microsoft Excel. Special Publication Vol. 5. Berkeley Chronology Center, Berekeley, California.

Lyubetskaya, T., Ague, J.J., 2010. Modeling metamorphism in collisional orogens intruded by magmas: II. Fluid flow and implications for Barovian and Buchan metamorphism, Scotland. American Journal of Science 310, 459–491.

Mahalik, N.K., 1994. Geology of the contact between the eastern Ghats belt and North Orissa craton, India. Journal of the Geological Society of India 44, 41–51.

Mahapatro, S.N., Tripathy, A.K., Nanda, J., Roy, A., 2009. Coexisting ultramylonite and pseudotachylyte from the eastern segment of the Mahanadi shear zone, eastern Ghats Mobile Belt. Journal of the Geological Society of India 74, 679–689.

Mahato, S., Goon, S., Bhattacharya, A., Mishra, B., Bernhardt, H.J., 2008. Thermo-tectonic evolution of the north Singhbhum Mobile Belt (eastern India): a view from the western part of the belt. Precambrian Research 162, 102–127.

Maji, A.K., Goon, S., Bhattacharya, A., Mishra, A., Mahato, S., Bernhardt, H.-J., 2008. Proterozoic polyphase metamorphism in the Chhotanagpur gneissic complex (India), and implication for trans-continental Gondwanaland correlation. Precambrian Research 162, 385–402.

McQueen, D.M., Scharnberger, C.K., Scharon, L., Halpern, M., 1972. Cambro-Ordovician paleomagnetic pole position and rubidium-straontium total rock isochron for charnockitic rocks fromn Mirny station, east Antractica. Earth and Planetary Science Letters 16, 433–438.

Mehnert, K.R., 1972. Granulites. Results of a discussion II. Neues Jahrbuch. für Mineralogie –Monatshefte 1972, 139–150.

Mezger, K., Cosca, M., 1999. The thermal history of the eastern Ghats Belt (India), as revealed by U–Pb and 40Ar/39Ar dating of metamorphic and magmatic minerals: implications for the SWEAT hypothesis. Precambrian Research 94, 251–271.

Mikhalsky, E.V., 2007. Neoproterozoic and early Paleozoic geological complexes of eastern Antarctica: composition and origin. Moscow un. Geological Bulletin 62, 293–305.

Mikhalsky, E.V., Sheraton, J.W., Beliatsky, B.V., 2001. Preliminary U–Pb dating of Grove Mountains rocks: implications for the Proterozoic to early Palaeozoic tectonic evolution of the Lambert glacier–Prydz Bay area (East Antarctica). Terra Antarctica 8, 3–10.

Mishra, S., Gupta, S., 2014. Superposed deformation and inherited structures in an ancient dilational step-over zone: post-mortem of the Rengali Province, India. Journal of Structural Geology 59, 1–17.

Mishra, S., Deomurari, M.P., Wiedenbeck, M., Goswami, J.N., Ray, S., Saha, A.K., 1999. ^{207}Pb/^{206}Pb zircon ages and the evolution of the Singhbhum craton, eastern India: an ion microprobe study. Precambrian Research 93, 139–151.

Misra, S., Moitra, S., Bhattacharya, S., Sivaraman, T.V., 2000. Archean granitoids at the contact of eastern Ghats granulite belt and Singhbhum-Orissa craton, in Bhubaneswar-Rengali sector, Orissa, India. Gondwana Research 3, 205–213.

Mohanty, S.P., 2015. Palaeoproterozoic supracrustals of the Bastar Craton: dongargarh supergroup and sausar group. In: Mazumder, R., Eriksson, P.G. (Eds.), Precambrian Basins of India: Stratigraphic and Tectonic Context. Geological Society of London Memoir Vol. 43, pp. 151–164.

Mojzsis, S.J., Devaraju, T.C., Newton, R.C., 2003. Ion microprobe U–Pb age determinations on zircon from the late Archean granulite facies transition zone of southern India. Journal of Geology 111, 407–425.

Montel, J.M., Foret, S., Veschambre, M., Nicollet, C., Provost, A., 1996. Electron microprobe dating of monazite. Chemical Geology 131, 37–53.

Mukhopadhyay, A.K., Bhattacharya, A., 1997. Tectonothermal evolution of the gneiss complex at Salur in the eastern Ghats Granulite Belt of India. Journal of Metamorphic Geology 15, 719–734.

Nash, C.R., Rankin, L.R., Leeming, P.M., Harris, L.B., 1996. Delineation of lithostructural domains in northern Orissa (India) from Landsat thematic mapper imagery. Tectonophysics 260, 245–257.

Newton, R.C., Perkins III, D., 1982. Thermodynamic calibration of geobarometers based on the assemblages garnet–plagioclase–orthopyroxene (clinopyroxene)–quartz. American Mineralogist 67, 203–222.

Northrup, C.J., 1996. Structural expression and tectonic implications of general noncoaxial flow in the midcrust of a collisional orogen: the northern Scandinavian Caledonides. Tectonics 15, 490–505.

Olsen, T.S., Kohlstedt, D.L., 1985. Natural deformation and recrystallization of some intermediate plagioclase feldspars. Tectonophysics 111, 107–131.

Paces, J.B., Miller Jr., J.D., 1993. Precise U–Pb ages of Duluth complex and related mafic intrusions, northeastern Minnesota: new insights for physical, petrogenetic, paleomagnetic and tectono-magmatic processes associated with the 1.1 Ga midcontinent rift system. Journal of Geophysical Research 98, 13997–14013.

Pandey, B.K., Prasad, R.N., Veena, K., Sagar, S., Gupta, J.N., Saraswat, A.C., 1989. Early Proterozoic Rb–Sr isochron ages for the granitic rocks from parts of Koraput district, Orissa, India. Indian Minerals 43, 273–278.

Panigrahi, M.K., Mookherjee, A., Pantulu, G.V.C., Gopalan, K., 1993. Granitoids around Malanjkhand copper deposit: types and age relationship. Proceedings of the Indian Academy of Sciences (Earth and Planetary Science) 102, 399–413.

Panigrahi, M.K., Misra, K.C., Bream, B., Naik, R.K., 2002. Genesis of the granitoid affiliated copper–molybdenum mineralization at Malanjkhand central India: facts and problems. Proc. 11th Quadrennial IAGOD Symposium and Geocongress, Windhoek, Namibia.

Passchier, C.W., Trouw, R.A.J., 1998. Microtectonics. Springer Verlag Berlin, Heidelberg and New York (ISBN 3-540-58713–6).

Paterson, S.R., Vernon, R.H., Tobisch, O.T., 1989. A review of criteria for the identification of magmatic and tectonic foliations in granitoids. Journal of Structural Geology 11, 349–363.

Phillips, G., Wilson, C.J.L., Campbell, I.H., Allen, C.M., 2006. U–Th–Pb detrital zircon geochronology from the southern Prince Charles mountains, East Antarctica — defining the Archaean to Neoproterozoic Ruker Province. Precambrian Research 148, 292–306.

Phillips, G., Kelsey, D.E., Corvino, A.F., Dutch, R.A., 2009. Continental reworking during overprinting orogenic events, southern Prince Charles mountains, East Antarctica. Journal of Petrology 11, 2017–2041.

Post, N.J., Hensen, B.J., Kinny, P.D., 1997. Two metamorphic episodes during a 1340–1180 Ma convergent tectonic event in the Windmill Islands, East Antarctica. In: Ricci, C.A. (Ed.), The Antarctic Region: Geological Evolution and Processes. Terra Antarctica Publications, Siena, pp. 157–161.

Prabhakar, N., 2013. Resolving poly-metamorphic Paleoarchean ages by chemical dating of monazites using multi-spectrometer U, Pb and Th analyses and sub-counting methodology. Chemical Geology 347, 255–270.

Prabhakar, N., Bhattacharya, A., 2013. Paleoarchean partial convective overturn in the Singhbhum craton, eastern India. Precambrian Research 231, 106–121.

Rasmussen, B., Muhling, J.R., 2007. Monazite begets monazite: evidence for dissolution of detrital monazite and reprecipitation of syntectonic monazite during low-grade regional metamorphism. Contributions to Mineralogy and Petrology 154, 675–689.

Rasmussen, B., Fletcher, I.R., McNaughton, N.J., 2001. Dating low-grade metamorphicevents by SHRIMP U–Pb analysis of monazite in shales. Geology 29, 963–966.

Rasmussen, B., Fletcher, I.R., Sheppard, S., 2005. Isotopic dating of the migration ofa low-grade metamorphic front during orogenesis. Geology 33, 773–776.

Rekha, S., Bhattacharya, A., 2013. Growth, preservation of Paleoproterozoic-shear-zone-hosted monazite, north of the western Dharwar craton (India),and implications for Gondwanaland assembly. Contributions to Mineralogy and Petrology 166, 1203–1222.

Rekha, S., Bhattacharya, A., 2014. Paleoproterozoic/Mesoproterozoic tectonism in the northern fringe of the western Dharwar craton (India): its relevance to Gondwanaland and Columbia supercontinent reconstructions. Tectonics 33, 552–580.

Rekha, S., Upadhyay, D., Bhattacharya, A., Kooijman, E., Goon, S., Mahato, S., 2011. Lithostructural and chronological constraints for tectonic restoration of Proterozoic accretion in the eastern Indian Precambrian shield. Precambrian Research 187, 313–333.

Rekha, S., Bhattacharya, A., Viswanath, T.A., 2013a. Microporosity linked fluid focusing and monazite instability in greenschist facies para-conglomerates, western India. Geochimica et Cosmochimica Acta 105, 187–205.

Rekha, S., Viswanath, T.A., Bhattacharya, A., Prabhakar, N., 2013b. Meso/Neoarchean crustal domains along the north Konkan coast, western India: the WesternDharwar craton and the Antongil-Masora block (NE Madagascar) connection. Precambrian Research 233, 316–336.

Rickers, K., Mezger, K., Raith, M.M., 2001. Evolution of the continental crust in the Proterozoic eastern Ghats Belt, India and new constraints for Rodinia reconstruction: implications from Sm-Nd, Rb–Sr and Pb–Pb isotopes. Precambrian Research 112, 183–212.

Sarkar, G., Gupta, S.N., 1990. Dating of early Precambrian granite complex of Bastar district, Madhya Pradesh. Records of the Geological Survey of India 123, 31–33.

Sarkar, S.N., Gopalan, K., Trivedi, J.R., 1981. New data on the geochronology of the Precambrians of Bhandara-drug, Central India. Indian Journal of Earth Sciences 8, 131–151.

Sarkar, G., Corfu, F., Paul, D.K., Mcnaughton, N.J., Gupta, S.N., Bishui, P.K., 1993. Early Archaean crust in Bastar craton, Central India — a geochemical and isotopic study. Precambrian Research 62, 127–137.

Schärer, U., de Parseval, P., Polve, M., de Saint Blanquat, M., 1999. Formation of the Trimouns talc–chlorite deposits (Pyrenees) from persistent hydrothermal activity between 112 Ma and 97 Ma. Terra Nova 11, 30–37.

Selverstone, J., 1985. Petrologic constraints on imbrications, metamorphism and uplift in the SW Tauern window, eastern alps. Tectonics 4, 687–704.

Selverstone, J., Spear, F.S., Franz, G., Morteani, G., 1984. High pressure metamorphism in the SW Tauren window, Austrai: P–T paths from hornblende-kyanite–staurolite schists. Journal of Petrology 25, 501–531.

Sen, S.K., Bhattacharya, A., 1984. An orthopyroxene-garnet thermometer and its application to the madras charnockites. Contributions to Mineralogy and Petrology 88, 64–71.

Sharma, M., Basu, A.R., Ray, S.L., 1994. Sm-Nd isotopic and geochemical study of the Archean tonalite-amphibolite association from the eastern Indian craton. Contributions to Mineralogy and Petrology 117, 45–55.

Simmat, R., Raith, M.M., 2008. U-Th-Pb monazite geochronometry of the eastern Ghats Belt, India: timing and spatial disposition of poly-metamorphism. Precambrian Research 162, 16–39.

Spear, F.S., 1989. Petrologic determination of of pressure–temperature–time paths. In: Spear, F.S., Peacock, S.M. (Eds.), Metamorphic Pressure–Temperature-Time Paths. Short Course in Geology. American Geophysical Union, Washington, pp. 1–55.

Spear, F.S., Cheney, J.T., 1989. A petrogenetic grid for pelitic schists in the system SiO–Al$_2$O$_3$–FeO–MgO–K$_2$O–H$_2$O. Contributions to Mineralogy and Petrology 101, 149–164.

Stein, H.J., Hannah, J.L., Zimmerman, A., Markey, R.J., Sarkar, S.C., Pal, A.B., 2004. A 2.5 Ga porphyry Cu–Mo–Au deposit at Malanjkhand, Central India: implications for late Archean continental assembly. Precambrian Research 134, 189–226.

Stipp, M., Stünitz, H., Heilbronner, R., Schmid, S.M., 2002. The eastern Tonale fault zone: a 'natural laboratory' for crystal plastic deformation of quartz over a temperature range from 250 to 700 °C. Journal of Structural Geology 24, 1861–1884.

Tullis, J., Yund, R., 1987. Transition from cataclasite flow to dislocation creep of feldspar: mechanisms and microstructures. Geology 15, 606–609.

Tullis, J., Yund, R.A., 1991. Diffusion creep in feldspar aggregates: experimental evidence. Journal of Structural Geology 13, 987–1000.

Upadhyay, D., 2008. Alkaline magmatism along the southeastern margin of the Indian shield: implications for regional geodynamics and constraints on craton–eastern Ghats Belt suturing. Precambrian Research 162, 59–69.

Upadhyay, D., Raith, M.M., 2006. Intrusion age, geochemistry and metamorphic conditions of a quartz-monzosyenite intrusion at the craton–eastern Ghats Belt contact near Jojuru, India. Gondwana Research 10, 267–276.

Upadhyay, D., Raith, M.M., Mezger, K., Bhattacharya, A., Kinny, P.D., 2006. Mesoproterozoic rifting and pan-African continental collision in south- eastern India: evidence from the Khariar alkaline complex. Contributions to Mineralogy and Petrology 151, 434–456.

Wang, Y., Liu, D., Chung, S.-L., Tong, L., Ren, L., 2008. SHRIMP zircon age constraints from the Larsemann Hills region, Prydz Bay, for a late Mesoproterozoic to early Neoproterozoic tectono-thermal event in East Antarctica. American Journal of Science 308, 573–617.

Whitney, D.L., Teyssier, C., Fayon, A.K., Hamilton, M.A., Heizler, M., 2003. Tectonic controls on metamorphism, partial melting, and intrusion: timing and dura-tion of regional metamorphism and magmatism in the Nigde massif, Turkey. Tectonophysics 376, 37–60.

Wiedenbeck, M., Hanchar, J.M., Peck, W.H., Sylvester, P., Valley, J., Whitehouse, M., Kronz, A., Morishita, Y., Nasdala, L., Fiebig, J., Franchi, I., Girard, J.-P., Greenwood, R.C., Hinton, R., Kita, N., Mason, P.R.D., Norman, M., Ogasawara, M., Piccoli, P.M., Rhede, D., Satoh, H., Schulz-Dobrick, B., Skår, Ø., Spicuzza, M.J., Terada, K., Tindle, A., Togashi, S., Vennemann, T., Xie, Q. and Zheng, Y.-F., (2004). Further characterization of the 91500 zircon crystal. Geostandards and Geoanalytical Research 28, 9–39.

Williams, M.L., Hanmer, S., 2006. Structural and metamorphic processes in the lower crust: evidence from the East Athabasca mylonite triangle, Canada: a deep-crustal isobarically cooled terrain. In: Brown, M., Rushmer, T. (Eds.), Evolution and Differen-tiation of the Continental Crust. Cambridge Univ. Press, Cambridge, U. K.

Zhao, Y., Song, B., Wang, Y., Ren, L., Li, J., Chen, T., 1992. Geochronology of the late granite in the Larsemann Hills, East Antarctica. In: Yoshida, Y., Kaminuma, K., Shiraishi, K. (Eds.), Recent Progress in Antarctic Earth Science. Terra Science Publications, Tokyo, pp. 155–161.

Zhao, Y., Liu, X.H., Liu, X.C., Song, B., 2003. Pan-African events in Prydz Bay, East Antarctica, and its inference on East Gondwana tectonics. In: Yoshida, M., Windley, B.F., Dasgupta, S. (Eds.), Proterozoic East Gondwana: Supercontinent Assembly and Break-up. Geological Society of London Special Publications Vol. 206, pp. 231–245.